UNITED NATIONS UNIVERSITY

GEOTHERMAL TRAINING PROGRAMME
Orkustofnun, Grensásvegur 9,
IS-108 Reykjavík, Iceland

Reports 2010
Number 16

THE DOMES WELL FIELD AT OLKARIA, KENYA: RESERVOIR CHARACTERISTICS WITH EMPHASIS ON FLUID CHEMISTRY

Isaack K. Kanda
Geothermal Development Company - GDC
P.O. Box 17700
Nakuru – 20100
KENYA
isakandah@gmail.com

ABSTRACT

A total of 23 wells have now been drilled in the Domes Sector of the Olkaria geothermal system. Their current total steam yield is approximately 840 tons/hour which is sufficient to produce 120 MW of electric power. Data on the chemical composition of liquid water and vapour discharged from this well field have been used to reconstruct the composition and species distribution in the initial aquifer fluid using the Phase Segregation Model for wells with excess discharge enthalpy. The aquifer water is close to saturation with respect to calcite but under-saturated with fluorite except for the lowest temperature waters (~200°C). Aqueous carbon dioxide is either controlled by the close approach to equilibrium with specific hydrothermal mineral assemblages or source controlled i.e. by its flux from the magma heat source. The results for the other major reactive gases, hydrogen and hydrogen sulphide, show large scatter for their modelled concentrations in the initial aquifer fluid, making it difficult to deduce the processes that govern them. The collective use of geothermometers, measured well discharge enthalpy, subsurface pressure distribution, temperature build-up in wells after completion tests and circulation losses during drilling are weighed against spatial distribution of outputs in the well field. This has led to the development of a conceptual model that tends to sequestrate promising from non-promising areas. As the model demonstrates, well outputs are highest where reservoir pressures are highest and where the producing aquifers are deepest. A low-temperature zone runs north-south through the middle of the well field. In this zone, well discharges have liquid enthalpy. But discharge enthalpy increases both to the west and east, while good wells are observed to lie preferentially to the east of the cold zone. The proffered conceptual model suggests that new wells should be drilled in the southeast part of Domes.

1. INTRODUCTION

Detailed geological, geophysical and geochemical work at Olkaria geothermal area was conducted by different researchers during the period 1992-1993, with major highlights put on the Olkaria Domes. These early studies pioneered the institution of a working model that culminated in the sinking of the initial three exploration wells (OW-901, OW-902 and OW-903) for evaluating geothermal potential of the area. This resulted in a better understanding of the reservoir and the delineation of key structural

patterns in the area. Of the three wells, only OW-901 is to be used as a production well, whereas the other two, OW-902 and OW-903, are scheduled for injection/re-injection.

At the moment, at least 23 wells have already been drilled in an ongoing drilling program. These include: Wells OW-903A, 903B, 904A, 904B, 907A, 908, 908A, 909 and 910A which are planned for production, and wells OW-905A and 906A planned for injection and re-injection use, with depth variations targeting productive horizons up to 3000 m. Based on promising earlier yield results in terms of temperature and steam flow, a production well field of 7-8 km^2 was delineated in this area. This areal extent undoubtedly will change with time if a step-out well programme materializes, dependent on a satisfactory reservoir evaluation. From the available data, there is now adequate steam (in excess) at the wellhead to sustain a 120 MWe power plant. And, based on the stimulating results, the suggestion of erecting a 2×70 MWe power plant is, at present, a feasible near future step in Olkaria Domes, which will be successful if delineation of the reservoir is clearly revised and infill drilling of production wells is conducted. A combination of vertical and directional drilling has proved to be effective in the recent past and has enabled more than one well to be sunk in the same pad, hence abridging the cost of steam gathering systems, separators and other basic infrastructure, among others.

All things considered, the primary purpose in developing a geothermal reservoir for power production is to prove the presence of steam through drilling. The average yield or the average steam flow in individual wells varies between and within fields, and the primary target of any drilled well is a zone of high permeability. This report is based on collective interpretation of different types of well data from the Olkaria Domes geothermal field in Kenya. It incorporates data from chemical well data (counting geothermometers), circulation losses, together with temperature profiles and pressure build-ups in wells while heating up and until thermal stability is achieved. Interpretation of these data has led to the delineation of a conceptual model of the field.

2. GEOLOGICAL FEATURES

2.1 Location

The Olkaria geothermal prospect is located on the floor of the southern section of the Kenya rift, which is a part of the ~3,000 km long East African Rift System that runs from Afar triple junction at the Gulf of Eden in the North to Beira, Mozambique in the south (KenGen, 1998; see Figure 1). The prospect lies south of Eburru and west of Mt. Longonot, geologically situated within the Greater Olkaria volcanic complex. The field under current study, Olkaria IV (Domes) or the Domes well field is one of seven geothermal fields in the Greater Olkaria geothermal area (GOGA) which have proven to be economically utilizable for power production. It is the most south-easterly situated sector and one of the most promising fields presently under development. The field is westerly bound by the Hell's Gate – Ol'Njorowa Gorge and a ring of domes both to the east and to the south.

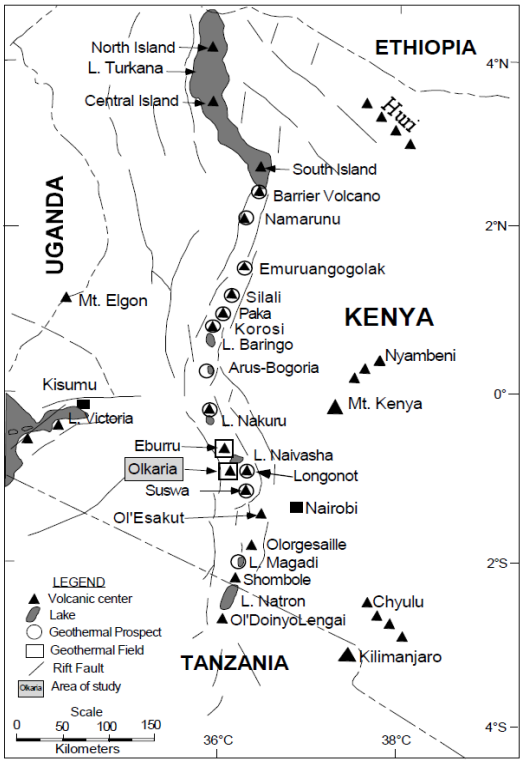

FIGURE 1: Map of the Kenya rift showing the location of Olkaria geothermal field and other Quaternary volcanoes along the rift axis (Lagat, 2004)

2.2 Regional geology

The evolution of the East African Rift has been discussed by many authors (e.g. Smith and Mosley, 1993; Baker et al., 1971, 1972; Smith, 1994; and Williams, 1972). The early evolution of the East African Rift was structurally controlled by rift faulting in a weak collisional zone at the contact between the Archaean Tanzania craton and Proterozoic orogenic belts. Activity within the Kenya rift started during late Oligocene (30 Ma) in the area referred to as the Turkana rift, but volcanism associated with the rift began later during Miocene, accompanied with domal uplift and vast ejection of phonolitic lava.

The sequential order of volcanism preceding major rift faulting laid down the idea that the driving force of the rifting process was provided by a convecting asthenospheric mantle (Baker et al., 1971). The Miocene volcanics were subsequently faulted, followed by a massive and extensive Pliocene eruption of trachytic ignimbrites in the central area, forming Kinangop and Mau tuffs. This eruption antedated the second faulting episode that gave rise to the formation of the graben structure of the rift valley, alongside fissure eruptions of trachytes, basalts, basaltic trachyandesites, and trachyandesites, which predated Quaternary volcanic activity of mafic to felsic composition.

2.3 Local geology

The surface geology of Olkaria volcanic complex has been described by MacDonald et al. (1987) as consisting of mildly peralkaline (comenditic) rhyolitic domes, lava flows, air fall pumices, and minor lake sediments, peripheral basalts and hawaiites. Quaternary comendites, pantellerites and an extensive cover of pyroclastic fall from the nearby Longonot and Suswa volcanoes envelop the surface to about 1400 m a.s.l., marked by structurally controlled volcanic eruption centres of Quaternary age, with Olkaria hill, Gorge Farm area and the Ololbutot fault zone being the most important volcanic centres. The latter correlates with the most recent volcanism, that resulted in a rhyolitic flow about 250 ± 100 years BP, as described by Omenda (1998) and Clarke et al. (1990).

Unlike other volcanic centres, Olkaria hill is not associated with an apparent caldera structure but an inference has been made with the presence of a ring of volcanic domes in the east and south, and a buried caldera in the southwest (Mungania, 1992; Clarke et al., 1990), bolstered by seismic wave attenuation studies (Simiyu et al., 1998). Another possible explanation for the ring structure is that it was produced by magmatic stress in the Olkaria 'magma chamber' with the line of weakness being the loci for volcanism (Omenda, 2000).

2.4 Lithostratigraphy (subsurface geology)

The subsurface geology of the Olkaria geothermal field has been divided into six broad lithostratigraphic groups by preceding authors based on age, tectono-stratigraphy, and lithology (Muchemi, 1999; Omenda, 1998). The formations in chrono-stratigraphical order from the oldest to the youngest include: The Proterozoic "basement" formations, the pre-Mau volcanics, the Mau tuffs, the Plateau trachytes, the Olkaria basalts and the Upper Olkaria volcanics.

Reflection seismic, gravity and geological correlations indicate that the depth to the "basement" is about 5-6 km in the Central Kenyan Rift (Simiyu and Keller, 1997). Similar studies done previously indicated the existence of a high-density magmatic intrusion into the metamorphic "basement" rocks (Baker and Wohlenberg, 1971). The "basement" is deemed to comprise Proterozoic amphibolite grade gneisses and schists and the associated marble and quartzite of the Mozambiquan group (Shackleton, 1986).

Pre-Mau formations are known to superimpose the basement and are composed of trachytes, basalts

and ignimbrites and are overlain by Mau tuffs of Pleistocene age, the latter of which forms the oldest rocks exposed in the Olkaria area, commonly in the area around Olkaria Hill (Omenda, 1994). The Pre-Mau formations vary in texture from consolidated to ignimbritic, and they are the main geothermal reservoir rocks in the Olkaria west field, as observed from drill chippings from the geothermal boreholes in the area (Lagat, 2004). Plateau trachytes are of Pleistocene age occurring from about 1000 m to more than 2600 m in depth (Ogoso-Odongo, 1986; Omenda, 1998), and they are encountered in the boreholes in the Olkaria area (Lagat, 1995). The Olkaria basalt, consisting of basaltic lava flows, minor pyroclastics and trachytes, with a total thickness variation that ranges from 100 to 500 m, is considered to act as a caprock for the Olkaria geothermal system (Ambusso and Ouma, 1991). The upper Olkaria formation occurs from the surface down to about 500 m depth and consists of comendite lavas and their pyroclastic equivalents, ashes from Suswa and Longonot volcanoes and minor trachytes and basalts (Clarke et al., 1990; Omenda, 1998).

2.5 Structural setting

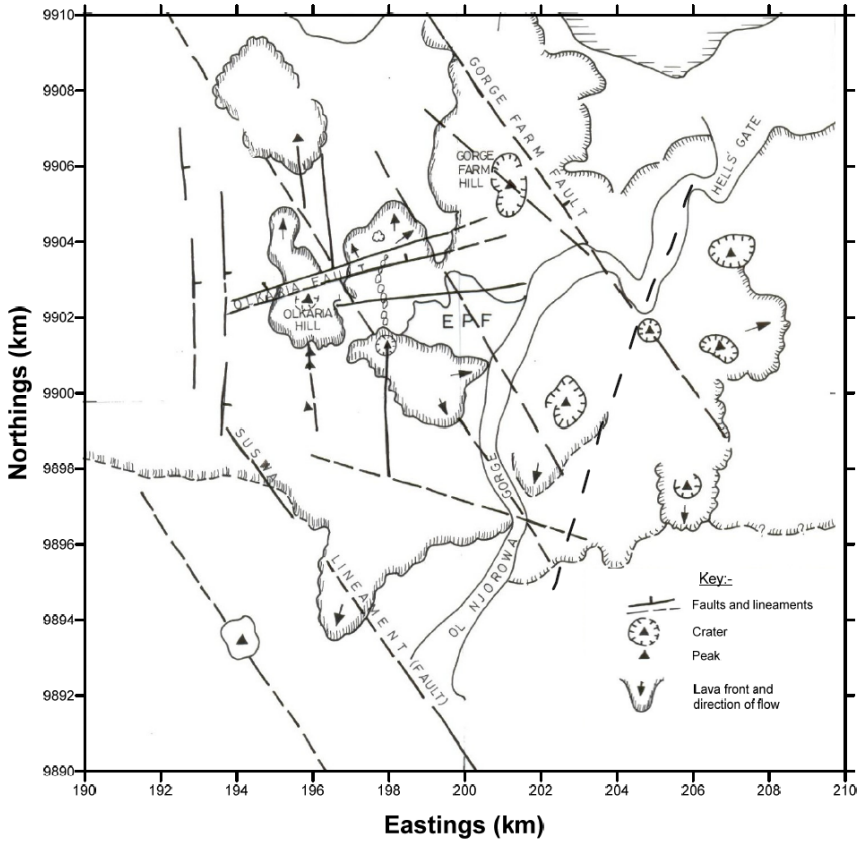

FIGURE 2: Structural map of the Greater Olkaria volcanic complex (adopted from Lichoro, 2009)

As described by Lagat (1995), the structures in the Greater Olkaria volcanic complex include the ring structure, the Ol'Njorowa gorge, the ENE-WSW Olkaria fault and N-S, NNE-SSW, NW-SE and WNW-ESE trending faults (Figure 2), being common phenomena in the East, Northeast and West Olkaria fields but are scarce in the Olkaria Domes area, probably due to the thick cover of pyroclastic material. Gorge Farm fault is probably the most prominent of these faults, bounding the geothermal fields in the northeast and extending to the Olkaria Domes area. NW-SE and WNW-SSW trending faults are believed to be the oldest and are associated with graben formation during rift development, whereas the most recent structures are the N-S and NNE-SSW trending faults (Lagat, 1995).

Hydroclastic craters located on the northern edge of the Olkaria Domes area are marked by magmatic explosions which occurred in submerged country, forming a row alongside which an extrapolated caldera rim trace passes (Mungania, 1999). The Ol'Njorowa gorge, which was developed by faulting (resulting in the touristic feature seen today), was mainly formed due to a catastrophic outflow of Lake Naivasha during its high stand (Clarke et al., 1990). Subsurface faults have been encountered in most of the Olkaria wells (Mungania, 1999; Lagat, 2004; KenGen, 2000).

3. CHARACTERISTICS OF THE OLKARIA IV (DOMES) RESERVOIR

The distribution of geothermal manifestations in the Domes geothermal well field is strongly interrelated with geological structures, illustrated by concentrated fumarolic activity along the ring structure on the eastern side of the field and along the N-S trending fault (Clarke et al., 1990; Mungania, 1992). The area is crisscrossed by faults and fractures as revealed by fault breccias, sheared zones and circulation losses experienced during drilling. The main feeders of geothermal fluids in the area seem to be fissure zones associated with subsurface faults and fractures, and contact zones between formations (Lagat, 2004).

From previous studies, the reservoir temperature in the Domes geothermal well field was estimated from temperature recovery tests, shut-in temperature profiles, hydrothermal alteration mineralogy and fluid inclusion measurements, indicating temperatures in excess of 340°C based on the initial three exploration wells (Lagat, 2004). From a geophysical perspective, the apparent existence of a high-resistivity core suggests reservoir temperatures that transcend 250°C (Lichoro, 2009), whereas solute and gas geothermometry from selected wells gave temperatures in the range of 250-350°C (Malimo, 2009).

Ofwona (2002) discussed and refined previous models by diverse authors and defined a working conceptual model for Olkaria West and East. In addition to the two upflow zones proposed in the earlier models for Olkaria, the author proposed the possibility of a third upflow zone for the Domes well field. Based on fluid chemistry and the reservoir temperatures seen, it was suggested that Olkaria West, Olkaria Central, Olkaria Northeast/Olkaria East and Olkaria Domes were separate systems, while insinuating the possible existence of a link between Olkaria East and the Domes well field. A detailed Domes well field reservoir assessment by Kariuki (2003), based on the initial three wells, indicated that the well field is a high-temperature resource with a large areal extent, although the actual size was not yet known. The author suggested that the upflow zone was somewhere on the northern or eastern side of well OW-903 with an outflow zone around well OW-902. The recommendations were then given that, while appraising the well field, more emphasis should be directed towards the north or eastern sides of well OW-903, in order to target the upflow area, and furthermore, that wells be cased deeper to seal off the cooler inflow at 1000 m a.s.l.

Generally in Olkaria, the pressure maxima are considered to represent major upflow zones of hot fluid, associated with the ENE-WSW trending Olkaria fault. However, there is a separate pressure high on the eastern part of the Olkaria Domes sector (Karingithi et al., 2010). The deep Olkaria geothermal reservoir is liquid-dominated, with most of the wells being two-phase in Domes, as indicated by the results from the depth penetrated by the deepest wells. The two-phase reservoir is overlain by a vapour-dominated steam cap (steam zone) with a temperature of about 240°C (Ambusso and Ouma, 1991). Aquifers in the Domes geothermal well field are marked by the presence of fractures and joints due to intrusions and are found along edges of plugs and domes, lithological contacts, joints, clast-matrix or fragment contacts in some breccias. Identification of permeable zones has been successfully interpreted by the use of loss or gain of circulation fluid, hydrothermal alteration mineralogical patterns, and temperature recovery test data (Lagat, 2004).

The compiled resistivity model from the 1-D inversions reveals that the Domes well field is generally characterized by a high-resistivity surface layer (> 100 Ωm) which is interpreted as fresh unaltered rocks, possibly due to the thick pyroclastic cover from the adjacent Longonot volcano. Below that is a low-resistivity layer of about 10 Ωm which correlates very well with the mineral alteration of the smectite-zeolite zone of the geothermal reservoir and this in turn overlays a high-resistivity core (> 50 Ωm) which is evident in all the cross-sections within the study area. Further down, at a few kilometres depth below sea level, a low-resistivity zone exists that could relate to the heat source for the geothermal system (Lichoro, 2009).

Geochemical assessment indicates that the excess enthalpy of well discharges at Olkaria is largely

produced by phase segregation, either by gravity under natural conditions (East sector) or in producing aquifers where extensive depressurizing boiling occurs (Karingithi et al., 2010). The initially drilled wells gave variable discharge enthalpy from 950 to 1850 kJ/kg. The first three wells (OW-901, OW-902 and OW-903), drilled for initial exploration to depths varying from 1900 to 2200 m (vertical wells), were sited to investigate the easterly, southerly and westerly extents of the reservoir and the structures that act as conduits for fluid flow into the field. Discharge tests revealed a mixture of sodium bicarbonate – chloride – sulphate water types with very dilute chloride concentrations ranging from 178 to 280 ppm (Opondo, 2008).

4. DATA SOURCE AND HANDLING

4.1 Data source

Until recently, Kenya Electricity Generating Company (KenGen) was solely responsible for well testing in the Domes area, so the data used in this report was made available by KenGen. The data consists of the analysis of water and steam samples collected at the well head, temperature and pressure logging during well build-up subsequent to a completion test, and partial data on circulation losses during drilling.

For the purposes of this report, data were admitted from particular wells. The assessed analytical data was taken from wells OW-901, OW-902, OW-903A, OW-903B, OW-904B, OW-905A, OW-906A, OW-908A and OW-909. The data include B, SO_4, Cl, F, CO_2, H_2S, SiO_2, Ca, Na, K and Mg from the water phase and CO_2, H_2S, CH_4, H_2 and N_2 from the gas phase. Other properties utilized were measured pH, total dissolved solids (TDS), gas sampling pressure (GSP) and enthalpy (H). Pressure and temperature logs from wells OW-903B, OW-904B, OW-905A, OW-906A, OW-907A, OW-908, OW-909A, OW-910A, OW-911A, OW-912, OW-913A, OW-914, OW-915A and OW-916 were also obtained.

4.2 Data screening

Out of the raw data from the aforementioned wells, singling out suitable analytical data that would best represent the aquifer temperature was done based on some important aspects. Some of the deliberated properties included ionic balance and the difference in quartz and Na/K geothermometer temperatures. The selected geothermometers, as well as ionic balance, were calculated with the aid of the WATCH chemical speciation program. The data displayed great discrepancies in both ionic and geothermometer values. For the ions, values $\leq 10\%$ were preferable, and for the geothermometers, a difference of maximum 20°C was accepted taking into account the general quality of available data.

A different approach considered trend consistencies for analytical data in relation to other data from the same well, and correlated them with more wells in the same field. This approach was presumed to eliminate unwarranted noise that might have arisen during the collection and analysis of samples. Tendencies for stability in enthalpy values as well as fluid composition boosted the reliability of the selected samples. Pressure and temperature downhole logs were selected based on how they approached stability. For this study, the established pressure build-ups within a well were inferred by clearly seen pivot points or zones, whereas temperatures were evaluated with reference to their advance towards the boiling point with depth.

4.3 Correction of measured pH

Good pH measurements from analytical results are critical in order to restore the chemical

composition and the speciation distribution of the aquifer fluid, which is essential for a reliable geochemical interpretation. This is true especially for assessing the state of mineral-solution equilibria for minerals with pH-dependent solubility, and also for mineral-gas equilibria involving CO_{2aq} and H_2S_{aq} irrespective of their solubility dependency. The reason is based on the hypothesis that aquifer pH affects the relative concentrations of carbonate and sulphide-bearing species (Karingithi et al., 2010; Gudmundsson and Arnórsson, 2005). High-temperature geothermal waters are usually pH-buffered by monomeric silica that forms a weak acid in water with a log K value of about -9.9 at 25°C (Busey and Mesmer, 1977; Arnórsson et al., 1982). The unionized monomeric silicic acid is partly removed from the solution during polymerization, causing an increase in solution pH, with the exception of waters that are predominantly pH-buffered by other weak acids (Gunnarsson and Arnórsson, 2005). In such high-temperature systems, aqueous concentrations are controlled by temperature dependent quartz (Angcoy and Arnórsson, 2010; see Figure 3).

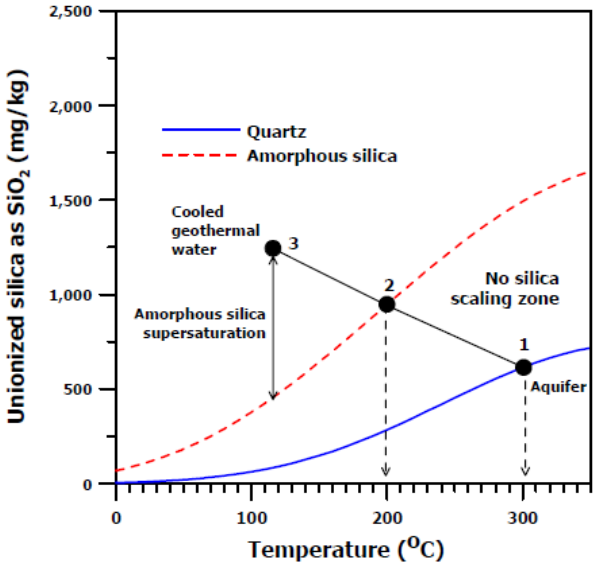

FIGURE 3: Solubility curves of quartz and amorphous silica as a function of temperature (Angcoy and Arnórsson, 2010)

For pH accuracy assurance, corrections were made based on the assumptions/possibility that pH measurement might have been delayed, a phenomenon commonly experienced during geothermal chemical analysis. Such delays would allow silica polymerization prior to pH measurement and hence paving the way for eventual misleading pH readings. Polymerization may change the water pH depending on what the initial pH was before the onset of polymerization by either the removal of monomeric silica (weak acid) from the solution, which tends to increase pH, and by the formation of oligomers (stronger acids), thus tending to decrease the pH, as discussed by Tossell and Sahai (2000). Consequently, above a pH of ~9, the removal of silica monomers dominates the pH change over oligomer formation because, at this high pH, a significant fraction of the dissolved silica is ionized (Karingithi et al., 2010).

Corrections of pH followed an iteration procedure that utilized the capabilities of the WATCH chemical speciation program version 2.4 (Bjarnason, 2010), a program based on thermodynamic data from the original program described by Arnórsson *et al.* (1982); it incorporates water sample analytical data and pH, assuming a liquid phase (without a gas phase), set water enthalpy and aquifer temperature (from geothermometers). The WATCH program only considers monomeric silica (Karingithi et al., 2010) for reasons discussed in Gunnarsson and Arnórsson (2005). Zotov and Keppler (2002) determined that dissolved silica in typical conditions of geothermal reservoir waters (< 600°C, 6-8 kbar) were all in monomeric form (monosilicic acid), $H_4SiO_4^o$. A monomer may also be written as $Si(OH)_4^o$ showing a central Si atom with 4 separate bonded –OH , or silinol, groups. The silinol groups between two monomers form the Si-O-Si bonding into dimers, an initial step called a condensation reaction towards the formation of higher molecular weight polymers (Angcoy and Arnórsson, 2010) as shown in Equation 1 below:

$$Si(OH)_4^o + Si(OH)_4^o \leftrightarrow (HO)_3\,Si - O - Si(OH)_3 + H_2O \quad (1)$$

Monomeric silica is calculated using measured pH values together with measured silica, the resulting speciation output of monomers is summed up to give total masses in moles and iterated using different pH values until the speciation masses of both measured (i.e. total dissolved silica) and monomeric silica tally to give the respective aquifer pH (i.e. calculated pH). Table 1 shows calculated versus measured pH alongside calculated monomeric silica.

TABLE 1: Calculated pH versus aquifer pH alongside monomeric silica of selected wells

Wells	Calculated pH	Aquifer pH	Monomeric silica
OW901	8.88	8.06	122
OW902	9.08	7.98	115
OW903A	9.1	7.95	108
OW903B	8.55	7.91	122
OW904	9.26	8.28	151
OW905	9.62	7.25	137
OW906	9.54	7.72	126
OW907	9.25	7.48	121
OW908	8.99	7.76	183
OW909	8.7	8.37	279

4.4 Calculation of aquifer fluid composition

The calculation of the aquifer fluid composition is based on a model discussed by Arnórsson et al., 2007; 2010), and was done with the help of the WATCH chemical speciation program. The calculations are based on the idea that the excess enthalpy from the field resulted from phase segregation, which occurred at 180°C (10 bars) and that the fluid was represented by liquid water only (Karingithi et al., 2010). The model of phase segregation is discussed in Arnórsson et al. (2010) as model 3 (see Figure 4), and brings into focus two versions of the model. The first version was adopted in this study, and is based on selecting a phase segregation temperature. It was also assumed that the vapour fraction in the initial aquifer fluid is zero. The second version of model 3 utilizes a vapour fraction derived from the H_2S and H_2 concentrations in the initial well discharge. The aquifer temperature is selected based on quartz and Na/K geothermometers results.

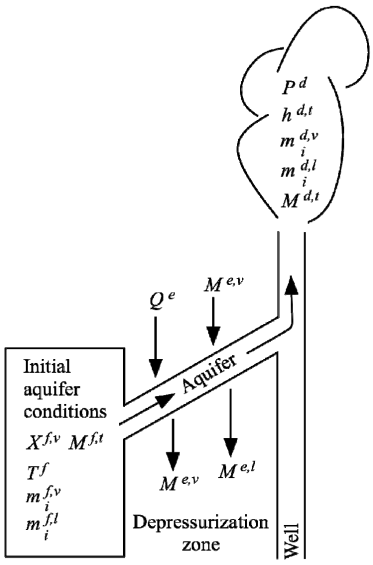

FIGURE 4: Schematic diagram describing the processes occurring in the depressurization zone around wells (Arnórsson et al., 2010)

The model of choice utilizes the vapour fraction in the initial aquifer fluid, i.e., the fluid beyond the depressurization zone around wells, which is given by an enthalpy conservation equation below (see Equation 2):

$$X^{f,v} = \frac{h^{f,t} - h^{f,l}}{h^{f,v} - h^{f,l}} \qquad (2)$$

where $X^{f,v}$ is the initial vapour fraction in the aquifer fluid, and h denotes specific enthalpy (kJ/kg). The superscript f designates the initial aquifer fluid, whereas t, l and v denote total fluid, liquid water and vapour, in that order.

The calculation involves two steps. The first step entails the calculation of the composition and speciation of the vapour and liquid at 180°C from selected analytical wellhead data of the water and steam samples as discussed in Arnórsson and Stefánsson (2005). This step uses measured enthalpy, ambient temperature, and corrected pH (see Section 4.3). The second step uses the WATCH output from the first run, that is the water chemical composition and the pH at 180°C (equivalent to 10 bar absolute vapour pressure) to calculate the composition and speciation distribution in the initial aquifer liquid water, taking the average of Na/K and quartz geothermometer temperatures to represent the initial aquifer liquid conditions.

4.5 Thermodynamic data, mineral solubility constants and saturation

Equilibrium constants were used for mineral assemblages, which potentially could control the concentrations of CO_2, H_2 and H_2S, to assess to what extent mineral-reactive gas equilibria could be approached in the aquifer (Table 2).

TABLE 2: Temperature equations for the equilibrium constants for mineral assemblage reactions that might control gas aqueous CO_2, H_2 and H_2S concentrations; the equations are valid in the range 0-350°C at $P_{sat.}$; unit activity was selected for all minerals and liquid water

Species activity	Reaction	Log K(T)
1. CO_2	$\frac{2}{5}czo + cal + \frac{3}{5}qtz = \frac{3}{5}gro + \frac{1}{5}H_2O\ (l) + \ CO_2\ (aq)$	-1.449-40536/T^2-2135.9/T + 0.0065639T +0.000002725T^2-0.193log(T)+0.1398
2. CO_2	$czo + cal + \frac{3}{2}qtz + \ H_2O(l) = \frac{3}{2}pre + \ CO_2\ (aq)$	-0.89+7251.5/T^2-1710.6/T+0.004188T + 0.000002683T^2-0.064log(T)
3. H_2S	$\frac{2}{3}gro + \frac{1}{3}pyr + \frac{1}{3}pyrr + \frac{2}{3}qtz + \ \frac{4}{3}H_2O(l) = \frac{2}{3}epi + \frac{2}{3}wol + H_2S\ (aq)$	13.659+555082/T^2-9256.6/T-0.043608T +0.000028613T^2+5.148log(T)-0.4014
4. H_2S	$\frac{1}{4}pyr + \frac{1}{2}pyrr + H_2O(l) = \frac{1}{4}mag + H_2S\ (aq)$	13.589+590215/T^2-9024.5/T-0.044882T +0.00002978T^2+5.068log(T)
5. H_2S	$\frac{1}{2}pyr + \frac{1}{2}mag + H_2O(l) = hem + H_2S\ (aq)$	14.340+630124/T^2-9605.6/T-0.047847T +0.000031589T^2+5.316log(T)
6. H_2	$\frac{3}{2}pyrr + H_2O(l) = \frac{3}{4}$pyr $+ \frac{1}{4}mag + H_2\ (aq)$	-1.654-95456.8/T^2-621.84/T-0.001257T +0.000007569T^2-0.6log(T)
7. H_2	$\frac{2}{3}gro + \frac{4}{3}pyrr + \frac{2}{3}qtz + \ \frac{4}{3}H_2O(l) = \frac{2}{3}epi + \frac{2}{3}wol + \frac{2}{3}pyr + \ H_2\ (aq)$	-1.544-151109/T^2-752.389/T-0.0005868T +0.00000708T^2-0.532log(T)-0.4014
8. H_2	$2mag + H_2O(l) = 3hem + H_2\ (aq)$	-2.257-111652/ T^2-1000.6/T-0.0012114T +0.00000799885 T^2-0.788log(T)

The source of the thermodynamic properties of $CO_{2(aq)}$, $H_{2(aq)}$ and $H_2S_{(aq)}$ is from Karingithi et al. (2010).

The saturation state of the aquifer water for selected hydrothermal minerals was also considered for calcite and fluorite. The thermodynamic values and properties for $CO_{2(aq)}$, $H_{2(aq)}$ and $H_2S_{(aq)}$ were retrieved from Fernandez-Prini et al. (2003), Holland and Powell (1998) and Robie and Hemingway (1995), respectively, as summed up in Karingithi et al. (2010).

5. SELECTED CHEMICAL FEATURES OF RESERVOIR FLUIDS

In order to understand the chemical evolution of any hydrothermal fluid and assess the state of equilibrium with regard to certain chemical reactions, some essential aspects need to be considered. These include the primary chemical composition data from well discharges, the concept of local equilibrium within the larger open geothermal system, modelling of aquifer fluid compositions and thermodynamic data on gases, aqueous species and minerals. This section presents key aquifer chemical characteristics, reactive gases (CO_2, H_2S and H_2), and mineral-solution equilibria for two selected minerals (calcite and fluorite).

5.1 Main chemical characteristics

The chemical concentration in the aquifer water varies from element to element (see Table 3). There exist, as well, notable differences in chemistry between aquifer and discharge wellhead waters with a general increase in the concentration of most elements at surface conditions.

TABLE 3: Calculated composition of the initial aquifer fluid produced from wet-steam wells, alongside enthalpy, aquifer temperature and pressure; chemical concentrations are in mg/kg.

	OW901	OW902	OW903A	OW903B	OW904B	OW905A	OW906A	OW907A	OW908A	OW909
$h^{f,t}$	925	843	967	911	958	911	1253	1402	1062	1391
T^{f}	216	198	225	213	223	213	283	310	245	308
T^{e}	180	180	180	180	180	180	180	180	180	180
$P^{,e}$	10	10	10	10	10	10	10	10	10	10
pH	6.87	6.86	6.94	6.65	7.23	5.97	6.89	6.87	6.52	7.73
SiO_2	497.0	269.3	287.9	216.7	464.7	367.4	520.3	614.2	382.8	598.8
B	1.20	1.26	0.94	0.87	1.67	0.04	3.96	0.88	1.53	3.04
Na	403	347	261	496	405	366	326	331	400	578
K	37	36	43	81	50	37	69	62	68	220
Ca	0.03	-	4.85	1.32	0.71	2.33	0.25	0.03	0.36	0.06
Mg	0.12	-	0.45	-	-	-	0.16	0.16	-	-
CO_2[a]	1418	956	380	1412	849	4061	2032	4693	4641	2890
H_2S[b]	11.6	1.0	1.0	2.2	8.2	0.9	31.4	13.4	0.7	24.2
SO_4	109.6	29.5	243.2	387.0	202.8	341.9	118.3	129.8	75.6	27.8
Cl	152	157	230	183	200	159	867	257	222	466
F	57	37	11	58	45	52	24	60	53	176
H_2	0.39	-	1.00	0.07	0.24	-	0.03	6.66	0.10	1.96
CH_4	0.94	0.20	3.87	2.42	0.63	3.73	-	5.13	0.76	2.91
N_2	46.1	7.0	281.8	41.5	-	209.9	593.6	146.0	195.0	43.5

$h^{f,t}$: Initial aquifer enthalpy (kJ/kg); P^{e}: Phase segregation pressure (bar-a); T^{e}; Phase segregation temperature (°C); T^{f}: Aquifer temperature (°C) based on the results of the quartz and Na/K geothermometers;
[a]Total: Carbonate carbon as CO_2; [b]Total: Sulphide sulphur as H_2S.

The pH of aquifer fluids from selected wells correlates directly except for wells OW-904A and OW-909 which display considerably higher values. The pH values range between 5.97 and 7.73, displaying a near neutral average value at aquifer temperature. Liquid water enthalpies calculated for initial aquifer conditions were, by and large, below 1000 kJ/kg with the exception of waters from wells OW-906A, OW-907A, OW-908A and OW-909. Nonetheless, discharge enthalpies are in excess and correspond to a vapour-dominated system in terms of volume as opposed to the calculated water enthalpy of the aquifer. The increase is in the magnitude of 13 to 54% in measured enthalpy.

The aquifer fluid in Domes is characterized by Na-Cl-HCO_3 water types, where HCO_3 is taken as total carbonate carbon (TCC) and represented as CO_2. Cl concentrations in the aquifer vary from 152 to 867 mg/kg compared to HCO_3 (380 to 2333 mg/kg), an observable fact atypical to high-temperature geothermal systems. Such high HCO_3 values can either be indicative of a peripheral origin of the aquifer water or a high level of magma degassing giving rise to an elevated CO_2 flux. The latter was suggested by Karingithi et al. (2010) to be the basis of high HCO_3 at Olkaria West; thus, the maturity of these waters could not be categorized effectively based on the contents of contained anions.

Among the cations, Na depicts lofty values, i.e. 261-578 mg/kg, when compared to K, Ca and Mg. The average values for K, Ca and Mg are 70, 1.1 and 0.22 mg/kg, respectively. The amount of SiO_2 in the aquifer water varies from 216 to 614 mg/kg, increasing with the range from 13 to 40 % in discharge fluids.

5.2 Reactive gas compositions

Reactive constituents, also termed geoindicators as defined by Arnórsson (2000), include chemical and isotopic constituents that tend to equilibrate with other reactive constituents and/or minerals of the rocks in the geothermal systems. They provide essential information on the physical state of geothermal reservoirs such as temperature and steam-to-water ratio.

The concentrations of H_2S, H_2 and CO_2 in the initial aquifer fluid are presented in Figure 5. Two mineral assemblages were selected for CO_2 concentrations: assemblages 1 and 2 (see Table 2). Apart from three samples showing a scatter closely matching with the assemblages, the concentrations were generally higher, departing in average from 0.3 to 0.4 SI units with reference to clinozoisite-calcite-quartz-prehnite and clinozoisite-calcite-quartz-grossular, respectively. The CO_2 concentrations are extremely high and this can be attributed to a high flux of CO_2 from the magmatic source that hinders its close approach to local equilibrium with the mineral assemblages given. This process has been discussed by previous authors (Arnórsson et al., 2007; Karingithi et al., 2010; Arnórsson, 2010).

The aquifer waters are typically low in H_2S relative to the equilibrium of assemblages 3, 4 and 5 (see Table 2), with an average departure of -1.0, -0.7 and -0.5 SI units, respectively. However, assessing the waters from the aquifer separately revealed that three of the samples relate closely to the assemblages. It is likely that the relatively low amount of H_2S is due to oxidation or contamination of samples with atmospheric air. Although O_2 was not detected in these waters as reported in the discharge data, it may have been present initially but then destroyed upon sample storage by a reaction with H_2S in the alkaline medium of the NaOH-solution.

The H_2 concentrations in the calculated aquifer fluids display a significant scatter compared to CO_2 and H_2S. There is no apparent relationship between H_2 and the assemblages considered. On average, the departure of H_2 from mineral equilibrium assemblages 6, 7 and 8 were in the magnitude of -0.05, -0.4 and 1.2, respectively. A single sample showed a close relationship with the hem-mag assemblage, whereas the rest displayed indistinct dispersion across pyrr-pyr-mag and gro-pyrr-qtz-epi-wol-pyr mineral assemblages.

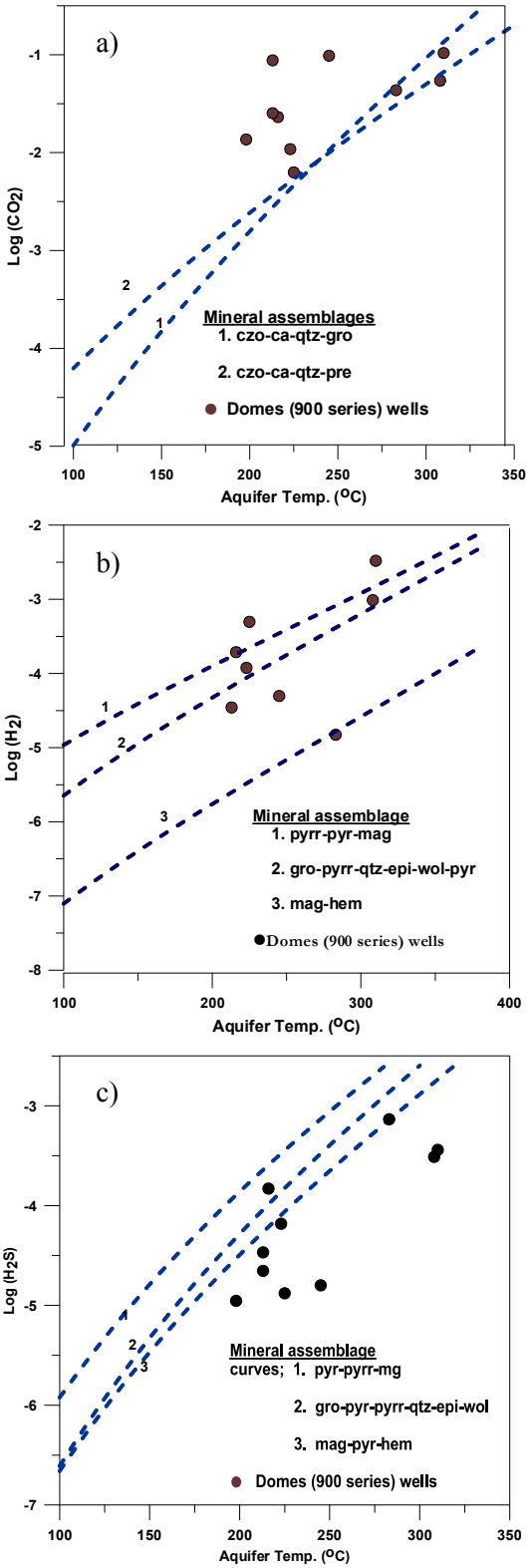

FIGURE 5: State of equilibrium between calculated concentrations of dissolved a) CO_2, b) H_2S and c) H_2 in the aquifer water of Olkaria wells with several minerals assemblages, as indicated; Table 2 displays the respective reactions and the temperature dependence of the equilibrium constants for these assemblages

5.3 Calcite and fluorite saturation

The ion activity product for calcite (Q) in aquifer waters of individual wells was scattered around the solubility constant for calcite, as seen in Figure 6. The average departure from the equilibrium was 0.07 log(Q/K) units and the standard deviation was 0.62 log(Q/K) units. However, some samples were far from being saturated, in particular well OW-901. The graph for fluorite shows that the aquifer waters of the lowest temperature were very close to fluorite saturation but hotter waters were under-saturated. In all of the aquifer waters considered for the present study, the dominant fluoride species was F^-. The other important F^-species was HF^o but it only constituted a small fraction of the dissolved F. The fluoride concentrations in the various aquifer waters were very variable. In view of the data on the F-species and the data for calcite, it was concluded that most of the aquifer waters modelled here are truly fluorite under-saturated.

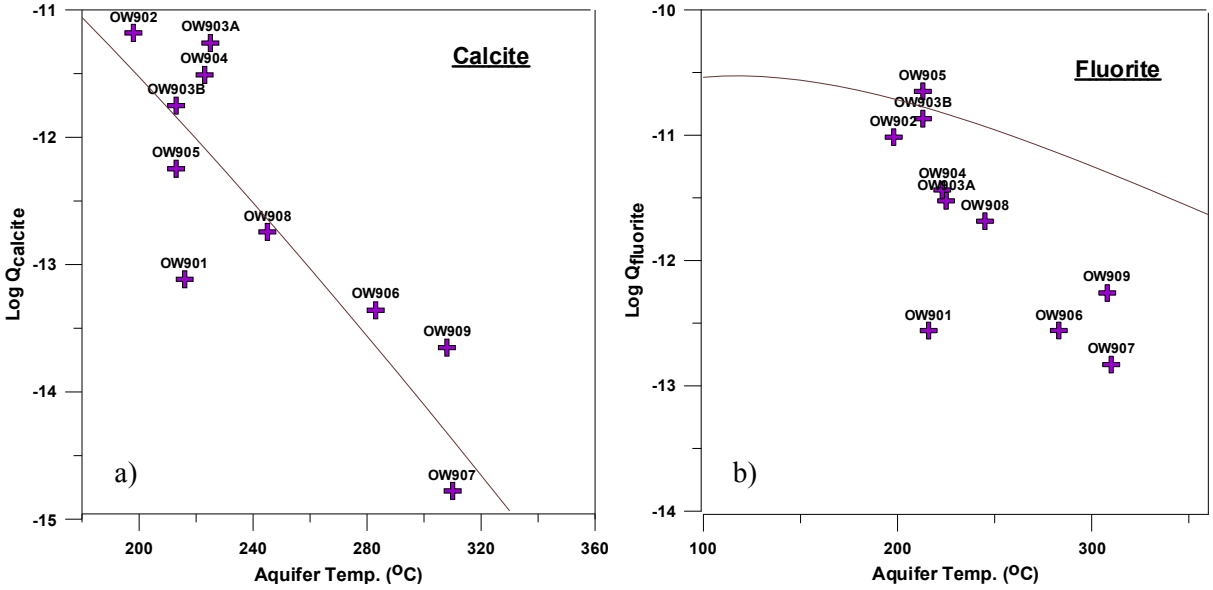

FIGURE 6: Saturation state versus aquifer temperature of a) calcite and b) fluorite minerals for Olkaria Domes waters

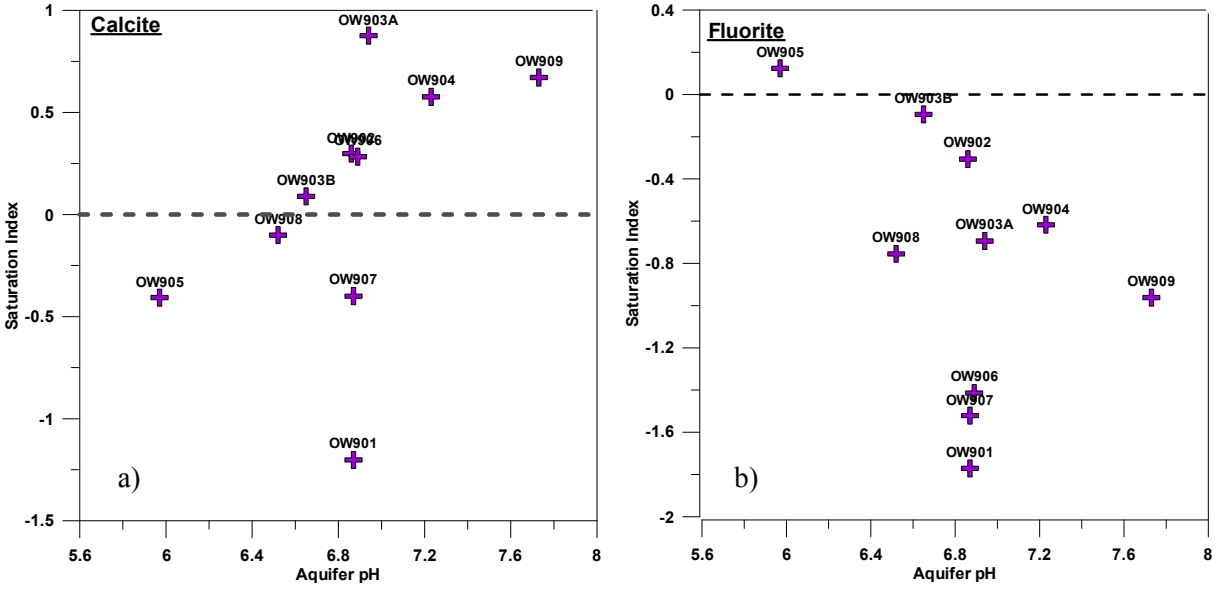

FIGURE 7: Saturation state versus aquifer pH of calcite and fluorite minerals for Olkaria Domes waters

LogQ values for calcite changed from under-saturation to over-saturation with increasing aquifer water pH (Figure 7). This change was not considered to be real, but rather an artefact reflecting an

error in the calculated aquifer water pH. Equilibration between aqueous solution and calcite is rapidly attained, certainly at the high temperatures of the Olkaria reservoir. The value calculated for aquifer water calcite saturation is dependent on several factors, largely the measured pH of water samples, and the analyzed concentrations of total carbonate carbon, also in water samples and the selection of aquifer water temperature. Errors in these parameters were also considered to be the cause of the observed relationship between the degree of calcite saturation and pH.

6. DEPTH LEVEL OF FEED ZONES

Understanding the depth level of feed zones and being able to clearly demarcate them is a very important step in delineating conceptual models of geothermal reservoirs. This section combines pressure and temperature (P & T) logs, circulation losses and geothermometers to establish such zones in Domes. Downhole pressure and temperature profiles obtained during the transient warm-up period of wells are a worthwhile investment, providing vital information that may no longer be available once the system has been altered by discharge.

6.1 Temperature logging

At the end of a completion test, the formations adjoining a well are comparatively cold. As the well warms up, the heat from the formation or aquifer may reach the well by conduction through the surrounding formation, direct inflow of fluid, convection cells within or flow directly across the well (Grant et al., 1982). The convective processes, prominent in permeable horizons, greatly outweigh conduction as a means of heat transfer. Because permeable zones are precisely those regions of the well where hot or cold fluid flows most readily, permeability usually shows up as a thermal anomaly, either hotter or colder, during temperature logging (Renner et al., 2007).

It is clear from the temperature logs that most of the discharged wells considered did not thermally stabilize at the end of downhole measurement (see Appendix I). The feed zones were evaluated based on the downhole temperature response to heating of the well. This assessment was done with reference to the boiling point curve as well as the ability of the runs to be consistent. The boiling point curve was drawn from the water table depth in respective wells and varied from 360 to 600 m with an average of 480 m below the surface. The water table depths were interpreted from pressure logs (see Table 4 and Appendix I).

The wells that approached thermal stability include wells OW-907A, OW-912, OW-914 and OW-915A. The rest of the wells were still approaching the state of stability by the time where the final runs were conducted. However, from the assessment, the majority of the wells are either sub-boiling or two-phase, as some wells had heated sufficiently to reach the boiling point curve.

6.2 Pressure logging

Pressure logs were used to identify pressure pivots in the well in order to recognize horizons that control well pressures, such as feed zones. At feed zones, there is direct contact between the well fluid and the reservoir, where the pressure in the well is equal to that at the same level in the reservoir (Grant et al., 1982) or where pressure equals the formation pressure (Leaver, 1986); this is referred to as a pivot point. As the well heats up, as Renner et al. (2007) put it, a transient decay of pressure build-up is caused by injection and the change in the gradient is caused by the warming of the water column in the well. Pressure pivots at the points where separate pressure runs converge. Elsewhere, the pressures in the well are set by the fluid in the well column. The gradient of the well, however, decreases as it warms up, indicating that the location is unequivocally identified by this pivot point.

TABLE 4: Temperature and pressure logs, geothermometers and circulation losses plus outputs for Olkaria Domes wells

WELL	MWe	Well depth (m)	Prod. casing depth (m)	Water table (m)	TQuartz (oC)	TNaK (oC)	Selected aquifer T (oC)	Geothermometer depth level (m)	Pivot points (m)	Aquifers from T logs (m)	Circ. losses	Selected aquifer depth (m)
OW-901	2.1	2200	nd	nd	234	209	222	nd	nd	nd	1100-1500	1300
OW-902	nd	2200	nd	500	222	188	205	700	none	1450	1300-1450, 1620-1680	1450
OW-903	nd	2200	nd	nd	225	195	210	nd	none	none	1539-1551, 1787-2027	ns
OW-903A	4.3	2801	nd	nd	206	239	223	nd	nd	nd	sporadic	ns
OW-903B	6.4	2793	1190	600	221	244	233	900	1050, 2000	1200	1540-1550, 1790-2030	1200
OW-904	5.5	nd	nd	nd	nd	nd	nd	nd	nd	nd	nd	ns
OW-904A	5.8	2799	nd	nd	nd	nd	nd	nd	nd	nd	sporadic	ns
OW-904B	4.9	2809	1204	400	249	255	252	850	1560	1250, 1900	sporadic	1560
OW-905A	0.0	2800	1269	500	204	203	204	700	1400	1400, 2600	sporadic	1400
OW-906A	1.0	2607	1259	500	289	262	276	1200	none	1800, 2600	nd	ns
OW-907A	8.6	2580	1250	500	305	256	281	1300	1500	1250, 1550	1204-1220, 1224-1252	1550
OW-908	4.1	2989	1250	500	342	300	321	2000	1500	1200, 1800	1288-1312	1500
OW-908A	7.0	2989	nd	nd	250	265	258	nd	nd	nd	sporadic	ns
OW-909	12.7	2989	nd	nd	263	358	311	nd	nd	nd	1834-1862, 2454-2472	ns
OW-909A	13.4	nd	903	600	nd	nd	nd	nd	2050	2150-2200	nd	2050
OW-910	nd	nd	nd	nd	nd	nd	nd	nd	nd	nd	nd	ns
OW-910A	13.4	2875	956	360	nd	nd	nd	nd	1900	1900, 2750	nd	1900
OW-911A	2.0	3000	951	500	nd	nd	nd	nd	1100	1100, 2600	970-978, 2876-2884	1100
OW-912	5.1	3010	856	400	nd	nd	nd	nd	1500	1500, 1800, 2200, 2900	nd	1500
OW-913A	0	nd	1200	400	nd	nd	nd	nd	none	1100, 2450, 2800	nd	ns
OW-914	5	nd	954	500	nd	nd	nd	nd	2000, 2550	1600, 2000, 2200	nd	2000
OW-914A	12	nd	nd	nd	nd	nd	nd	nd	nd	nd	nd	ns
OW-915A	13	2950	nd	500	nd	nd	nd	nd	1920, 2520	1150, 1900, 2500	nd	1900
OW-916	13	2980	nd	500	nd	nd	nd	nd	none	1350, 2700	nd	ns

(ns = not selected, nd = not detected and sporadic = irregularly distributed)

For some wells, pivoting was seen to occur between two or even more feed zones at depth (Table 4). The cause may be that different horizons have very similar pressure potentials. Shifting of pressure potential is also common and may result from reopening and closing effective aquifers. At Domes, the pivot horizons occurred at variable depths from as shallow as 1050 m to as deep as 2500 m below the surface. Where successive profile pivots depart from a common point, the last pivot point is selected if it is distinct, as an assumption, or else a simple average is applied.

6.3 Circulation losses/gains

Permeable zones in the field were also construed by loss or gain of circulation of drilling fluids. Data on circulation losses available for the present report were limited and unreliable, found only for wells OW-901, OW-902, OW-903, OW-904B, OW-907A, OW-908, OW-908A, OW-909, OW-911A and OW-912. They were limited in the sense that they were not sufficient for exhaustive spatial assessment, and unreliable in the sense that they were not reported alongside the drilling report. Drilling reports complement geological observations in evaluating circulation loss zones in that they give specific information on the depths where side valves were used, instead of drilling strings, to pump water through the annulus. This occurs generally during the change of drilling strings, bottom hole assemblies (BHA), or drillbits. Passage of water through the annulus and the time gap in between can destabilize formations and may lead to reopening of sealed feed zones which, in turn, can portray misleading impressions of circulation loss, bearing in mind that subsequent pumped water through the drill string will tend to refill these open aquifers (or cavities) before returning to the surface.

The data indicate some shallow permeable zones appearing to have been cased off. Circulation losses at shallow depths above the groundwater table are related to cold aquifers in comenditic lavas; whereas other feed zones are confined to lithological contacts between rock formations (Lagat, 2004). Certain permeable zones below the casing, suggested by circulation losses, are presented in Table 4.

6.4 Geothermometers

Temperature estimation in the earth's crust is usually based on temperature logs or heat flow gradient data (Spichak and Zakharova, 2009). The use of geothermometers and the heat flow gradient can help identify depth levels of dominating high-temperature aquifers based on the assumption that the temperature in the formation follows the boiling point curve with depth. Temperatures from geothermometers illustrated in this paper are as representative as possible of the average temperature of the sampled aquifer. Geothermometer results for the quartz and Na/K geothermometers and their respective depths obtained as part of this study are presented in Table 4. They were calculated using the WATCH chemical speciation program (Arnórsson *et al*., 1982), version 2.4 (Bjarnasson, 2010). These temperatures show a difference that goes beyond 100°C. The lowest aquifer temperature from a geothermometer reading is 204°C and the highest is 321°C, having an average of about 249°C. The depths of the aquifers based on geothermometer temperatures vary from 700 m to 2000 m.

6.5 Selection of main feed zones

The main aquifers in this study were identified by a combined use of temperature and pressure logs, circulation losses and geothermometers, with discussions limited to the available data. Two profile runs were carried out in well OW-902, and no pressure pivot was recorded. Data from thermal recovery suggest feed zones at depths of 1300 m and 1650 m which correspond to 150 and 60 m thick intervals of circulation loss, respectively, from geological observation. Geothermometer readings suggest an anomalously shallow aquifer depth of 700 m. In OW-901, the only available data were circulation losses from geological observation, typified by sporadic losses between depths of 1100 and 1500 m.

The pressure pivot in OW-903B showed a shift that started immediately below the casing, at about 1250 to 1950 m depth. Temperature logs supported the initial pivot zone at a depth of 1250 m whereas the geothermometer data suggested a depth of 900 m, which is inside the casing. A comparable shift was also observed in OW-904B with a budge from 1180 to 1950 m. However, there were no definite indications of main feed zones in the temperature logs. Geothermometer readings in this well suggested a feed zone location at 850 m depth which had been cased off. The indistinct pivot, at a depth of 1400 m for OW-905A, coincides with what seems to be a cold recharge zone which cools the well down and disappears into the formation again at 2600 m. The geothermometer suggested an aquifer depth of about 700 m. Well OW-906A had no pivot point, and though a zone of patchy losses was seen between depths of 1800 and 2600 m, and a geothermometer depth of 1200 m, the data was still inadequate for isolating any main feeding horizon.

In wells OW-907A, OW-908 and OW-912, pressure pivots occurred at a depth of about 1500 m. However, temperature logs for these wells differed. For 907A, a feeder zone from temperature logs of 1300 and 1550 m was suggested but, even though the pivot hinted a deeper feed zone, geological observation supported a shallow permeable zone through 44 m with losses of cuttings. The geothermometer depth matched, as well, with a depth of 1300 m. OW-908 indicated that the main feed zones were at 1200 and 1800 m and the pivots inclined to the average of these zones; however, a circulation loss interpreted from a geological perspective agreed with a feed zone at 1200 m depth, despite the 2000 m depth suggested by the geothermometer. Feed zones suggested by the temperature logs in well OW-912 were intermittent and started from 1500 m to the bottom of the well. Well OW-910A showed a well defined pivot at a depth of about 1920 m, matching the feed zone from thermal recovery data at 1900 m.

In well OW-909A, the pressure seemed to be pivoting at depths between 2000 to 2400 m below the surface, whereas temperature logs suggested a feed zone at a depth between 2150 m to 2200 m. There were no clear pressure pivots for wells OW-911A, OW-913A and OW-916. However, at a depth of 1100 m, an indistinct pivot was seen in OW-911A and corresponded to a feed zone suggested by

temperature logs. The feed zone indications from temperature log data for wells OW-913A and OW-916 could not help to draw conclusions on the dominant feed zones. Pressure pivots for wells OW-915A and OW-914, like some of the wells, were not stable, i.e., shifting from 2520 to 1920 m and from 2550 to 2000 m, respectively. However, some of the feed zones suggested from temperature logs coincided with the depth later obtained from pressure build-up.

7. CONCEPTUAL MODEL

The enormous upfront expense of developing heterogeneous reservoirs and the desire to increase ultimate outputs has spurred geothermal companies to develop and use innovative reservoir-characterization techniques. This could begin with a simplified conceptual model based on numerical simulation of the reservoir providing information on the economics and the development plan. This section describes a simplified conceptual model of the Domes well field utilizing the results discussed in the foregoing section (Chapter 6). The results used here were taken from preliminary observations and are limited to the available data. Although a few assumptions have been applied, much care was taken to ensure that the true natural state of the field was portrayed clearly. The data included well yields, geothermometers, feed-zone depths, measured discharge enthalpy and calculated aquifer pressures at 500 m a.s.l. The conceptual model discussed here complements the views expressed by preceding authors (e.g. Ofwona, 2002; Kariuki, 2003), in previous models of the well field and contiguous fields, refined and strengthened with added information acquired from the latest developments.

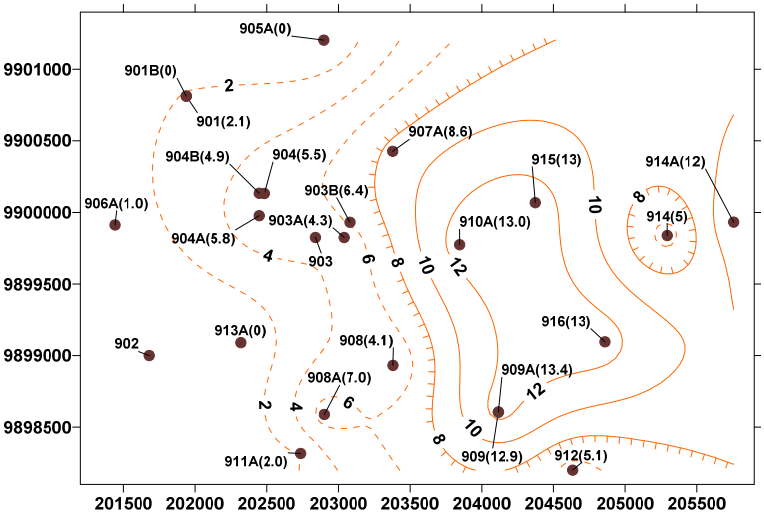

FIGURE 8: Measured well output distribution at the Domes well field. Numbers in parentheses indicate steam outputs expressed in MWe; the selected hatched isoline delineates low-production sections from high- ones

The graph for well output (Figure 8) is based on enthalpy and the total flow rate measurements of wells in Domes. This graph defines and grades the well field on the basis of well output. As the graph depicts, an easterly trending increase of outputs is evident. The areas to the west of wells OW-906A, OW-913A and OW-903B, and north of OW-905A seemingly comprise a dead-zone with no or low well yields. Other than OW-912 and OW-914, the eastern section of Domes has higher potential with performance in excess of 8 MWe per well. The vertical well OW-914 (5 MWe.) displays anomalously low values relative to its directional counterpart OW-914A (12 MWe) as well as to the general trend in the adjoining wells. The extent of this highly producing sector will be known when step-out wells are drilled. A trend line from OW-906A to OW-910A shows a 1 MWe increase in output per every 200 m surface distance. Figure 9 shows the output trend with an increasing number of wells being drilled. Apart from a few examples, steadiness in the increased output in the well field is seen to be intermittently altered whenever a well is drilled in the western part of the field. However, the consistent increase of the average output by the addition of wells is quite significant.

Geothermometers display a southerly increase in aquifer temperature in the northern section of the study area, and near wells OW-903A and OW-903B there is a distinguishable drop in temperature that extends southward to OW-902. However, a trend of temperature increase to the east and to the west

from OW-903A/B is evident (see Figure 10). The break in the trend around well OW-903 is an anomaly that is also evident in the outputs, enthalpy and geothermometer temperatures, and it seemingly demarcates two upflow zones. These upflow zones converge and merge in a northerly direction. It must be noted, however, that the plots are only suggestive due to constraints imposed by the data. The portrait exposed around well OW-906A is notably suspicious as it is supported by only one data point. More chemical data, especially for the most recently drilled wells on the eastern flank, will help to refine the model.

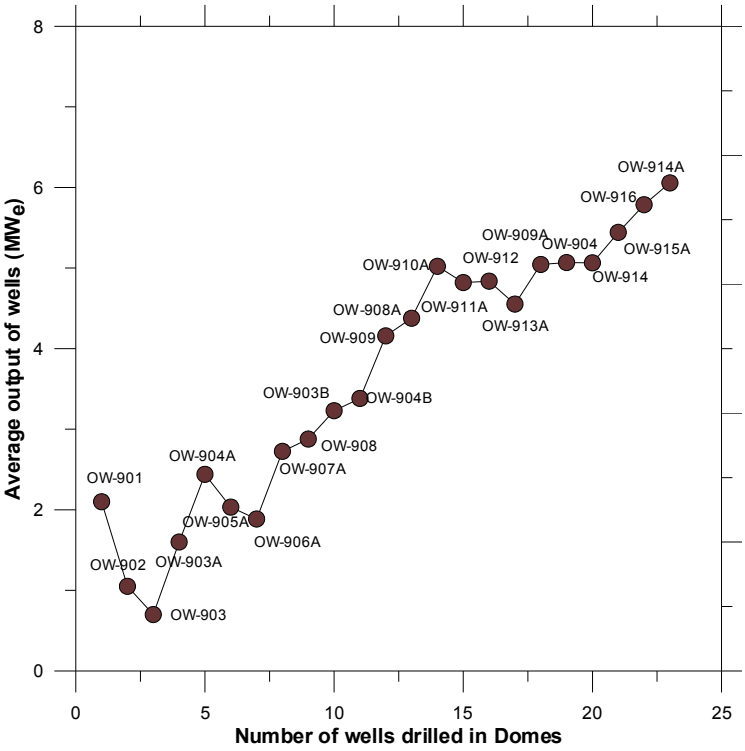

FIGURE 9: Average output of wells with number of wells drilled in Domes well field; the data used are presented in Table 4

Assuming that temperatures follow the boiling point curve with depth, the geothermometer temperature plots will help to suggest the distribution of the depth levels of the feed zones. The same trend is echoed by the selected aquifer depth levels displayed alongside geothermometers in Figure 10. The pattern displayed is definitive and rises to the east and west, corresponding to the relative rise in geothermometer temperatures, hence, depths at which the production of heated fluids in the aquifers is obtained. The outline reflects a scenario where the southeast section of the well field is an upflow zone with deeper aquifers. The availability of chemical data for wells OW-909A through OW-916 will serve to refine this hypothesis.

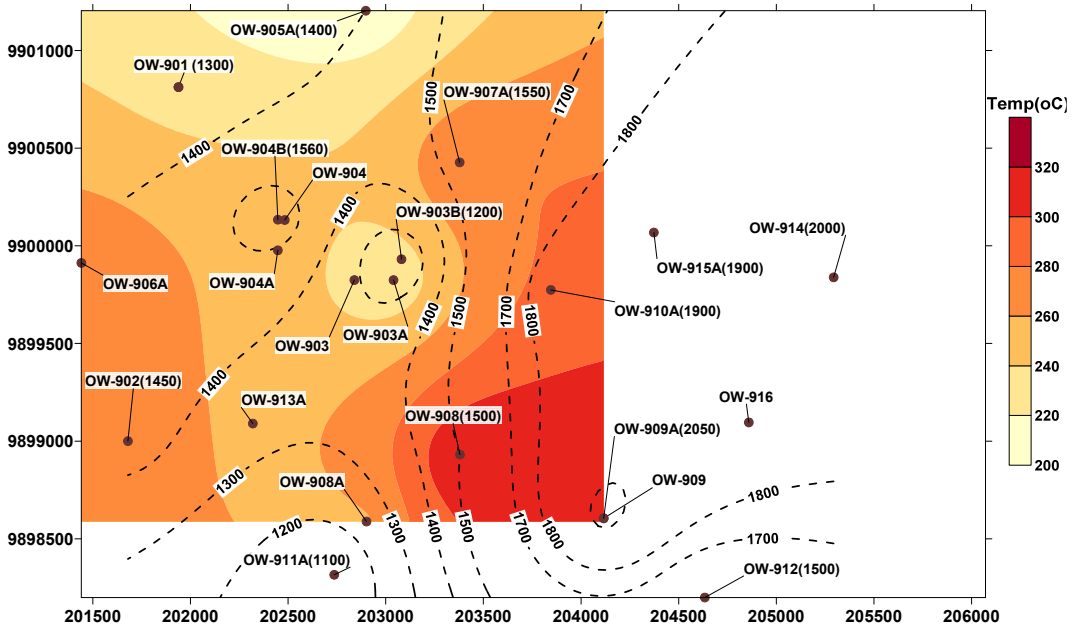

FIGURE 10: Aquifer temperatures according to geothermometers (coloured contour) and aquifer depth according to P & T logs, circulation losses and geothermometer depths (broken line contour) at the Domes well field; the corresponding temperatures and depths for respective wells have been put in parentheses

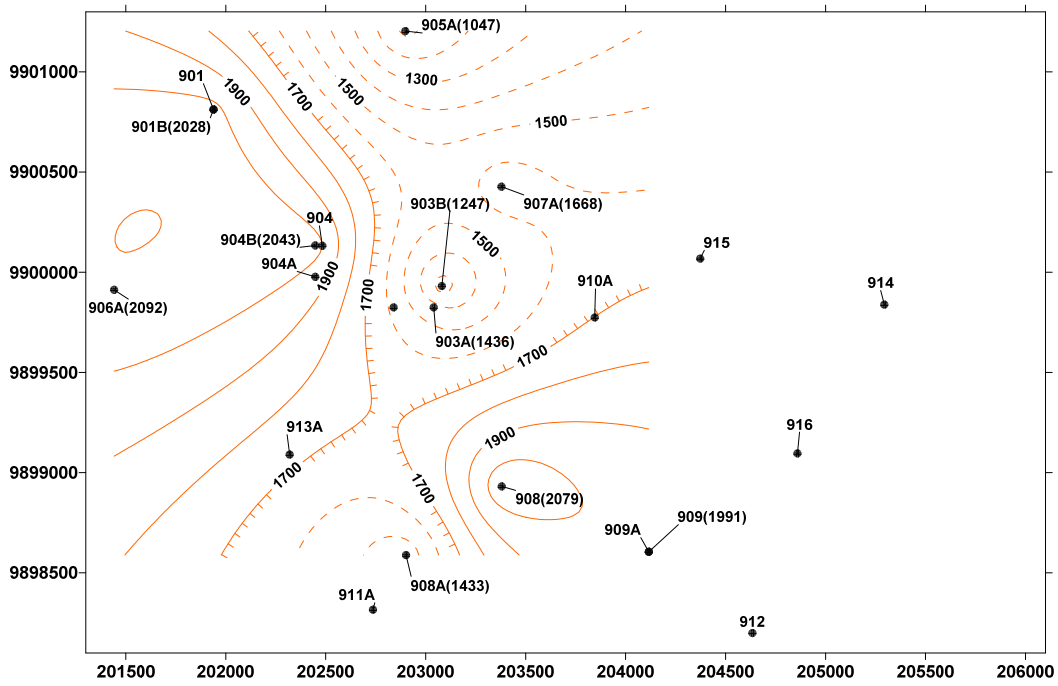

FIGURE 11: Measured discharge enthalpy of wells in Domes well field. Enthalpy values for individual well discharges are shown in parentheses; the hatched line at 1700 kJ/kg tends to separate low- from high-enthalpy areas

Figure 11 shows the distribution of well discharge enthalpies in Domes well field. The pattern of the iso-enthalpy lines is analogous to that for geothermometer temperatures with the low-enthalpy zone around well OW-903. The lowest enthalpy was observed at OW-905A (1047 kJ/kg) whereas the highest values were in OW-906A (2092 kJ/kg) and OW-908 (2079 kJ/kg) in the west and east, respectively. These ranges of enthalpy are equivalent to those of vapour-saturated liquid water between 243 and 372°C. For wells OW-905A and OW-903A/B, the liquid enthalpy suggested that the aquifer temperature is too low, insufficient to generate a large enough vapour fraction to immobilize the liquid. This low enthalpy is a cold zone, and runs north-south across the middle of the well field.

Pressures were calculated at 500 m a.s.l. in each well. These calculations were based on the measured pivot point pressure, assuming that the variation in pressure from this point to the 500 m a.s.l. reference depth level is determined by a column of liquid water that is at the boiling point at all depths. The results are shown in Table 5 below and presented graphically in Figure 12. These pressure variances were similarly reflected by geothermometers and enthalpy distribution. The low-pressure zone stretches across the middle of the well field, running approximately north-south through wells OW-913A, OW-908A, OW-911A, OW-903, OW-903A OW-903B and OW-907A, but a steady rise east of this zone was observed towards OW-914. The pressure at 500 m a.s.l. spanned from 80 to 110 bars. The results for wells OW-909A and OW-915A are not displayed due to a lack of directional drilling information crucial for depth adjustment.

TABLE 5: Calculated results for pressures at 500 m a.s.l.

Wells	Pivot level depth (m)	Well head elevation (m)	Corr. depth to 500 m a.s.l	T at pivot (°C)	P at pivot (bar)	Depth at T 500 m a.s.l (°C)	T at 500 m a.s.l (°C)	P at 500 m a.s.l (bar)
OW-903B	1156	2047	391	266	52	1011	296	81
OW-904B	1320	2004	184	303	90	1334	313	101
OW-905A	1327	1951	124	299	85	1194	306	93
OW-907A	1414	1975	61	295	80	1061	299	86
OW-908	1500	2019	19	303	90	1169	305	92
OW-910A	1812	1988	-324	328	125	1376	315	106
OW-911A	1040	1981	441	256	44	951	292	77
OW-912	1500	2075	75	299	85	1145	268	90
OW-914	2000	2010	-490	337	140	1410	318	110

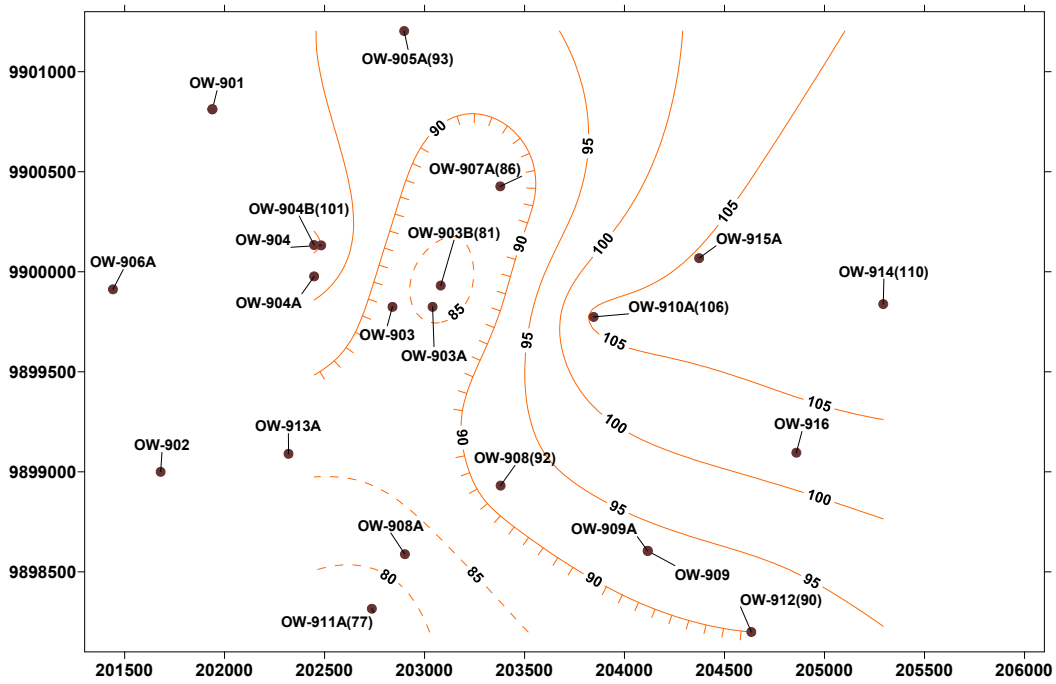

FIGURE 12: Calculated pressures in wells in Domes well field at 500 m a.s.l.; the numbers in parentheses by some wells indicate pressure in bar-a at 500 m a.s.l.

The collective use of geothermometers, selected producing horizons, measured well discharge enthalpy and subsurface pressure distribution from the selected reference depths, and reflected results on the output distribution have led to the construction of a conceptual model of the field. The picture suggests that producing horizons deepen towards the east and southeast segments of the well field and the deeper these producing horizons the better the outputs. The high pressure and high enthalpy correlate with high output. With this model, erection of a 2×70 MWe power plant within the well field becomes more likely; as the data already indicates that about 120 MWe (~80%) has been proven possible, and assuming a surplus of 10% as the trend suggests, then adding strategic wells in the eastern sector might bring the plan to fruition soon. A clear understanding of the main structures and their trends, and east-west mineral alteration (and thus temperature) variations across the well field would help define the reasons behind the low pressure and cold zone that runs north-south across the centre of the well field. The zone is most likely to be a downwarp that attracts inflow of cold recharge, hence, the anomaly.

8. SUMMARY AND CONCLUSIONS

Reservoir characterization encompasses all techniques and methods that improve our understanding of the geological, hydrological, geochemical, and petrophysical controls of fluid flow. It is a continuous process that begins with field discovery all the way to the last phases of production and abandonment. In Domes, the well field is presently under development for production, and a number of studies have already been carried out, as described in Chapter 3. However, as development progresses, the database is updated and so is our understanding of the reservoir. The main objective of this study was to add to the existing knowledge and, hence, improve on the current notes about the reservoir and its performance for economic purposes and planning sustainable development.

The data used in the present study were obtained from KenGen and include analytical results of water and steam samples collected at the wellhead, T & P logging during well build-up subsequent to completion tests, and data on circulation losses during drilling. Appropriate chemical data were

selected based on ionic balance and the agreement between the quartz and Na/K geothermometer temperatures. Calculations were carried out with the help of the WATCH chemical speciation program with tolerance values of ≤ 10% and ≤ 20°C, respectively. Trend consistency of analytical data from adjoining wells was also examined to get rid of any possible sampling and analytical errors. Pressure and temperature downhole logs were selected based on their approach to thermal stabilization. Established pressure build-up within a well was indicated by clear pivot points or zones, whereas temperatures were evaluated with reference to their approach to the boiling point curve.

Corrections for pH were made on the assumption that measurements might have been delayed. Such delays lead to polymerization of silica, which will eventually produce flawed pH results. Monomeric silica concentration was calculated using measured pH and by assuming that all dissolved silica in excess of amorphous silica solubility had polymerized at the time of pH measurement. Together with measured total dissolved silica and the preservation of alkalinity, the pH was calculated with the WATCH speciation program before the onset of silica polymerization. The measured pH so corrected was subsequently used to calculate aquifer water pH and mineral saturation. Correct pH is rather essential in modelling aquifer chemical composition; speciation distribution is essential for geochemical interpretation and assessing the state of mineral-solution equilibria for minerals with pH-dependent solubility, and also for mineral-gas equilibria involving CO_{2aq} and H_2S_{aq} irrespective of their solubility dependency. Correction of pH followed an iteration procedure that utilized the WATCH chemical speciation program to incorporate water sample analytical data and pH, assuming a liquid phase (without gas phase), water enthalpy and aquifer temperature (from geothermometers).

The initial aquifer fluids feeding Olkaria Domes well field were then modelled using the analytical data of the wellhead samples with, again, the aid of the WATCH chemical speciation program. As the fluid enthalpy assessment revealed, some of the wells in the field have liquid enthalpy, however, the majority of the wells have "excess enthalpy", meaning that the enthalpy of the well discharges is higher than that of liquid water at aquifer temperature. Geothermometer results indicated that the excess enthalpy of the well discharges was mainly produced by phase segregation in producing aquifers or occurred under natural conditions through the formation of a gravity induced steam zone. And since the reservoir is liquid-dominated, the excess enthalpy reflected a change in the enthalpy of the flowing fluid between initial fluids present at the aquifer and the wellhead. Calculation of the aquifer fluid component was, therefore, done based on the Phase Segregation Model (PSM) where phase segregation occurred at a temperature of 180°C (equal to 10 bar-a).

The stepwise approach of reinstating aquifer chemistry started with the calculation of the composition and speciation of the vapour and liquid at 180°C from the selected analytical wellhead data of the water and steam. This step used measured enthalpy, ambient temperature and corrected pH. The second step used the WATCH output from the first run that is the water chemical composition and the pH at 180°C (equivalent to 10 bar-a vapour pressure) to calculate the composition and speciation distribution in the initial aquifer liquid water, taking the average of Na/K and quartz geothermometer temperatures to represent the initial aquifer liquid temperature and enthalpy. With the initial aquifer fluid concentrations, the WATCH speciation program was used simultaneously to calculate individual species activities. The results of these modelled fluids were used to assess how closely the fluids had come to equilibrium conditions, with respect to various mineral-gas and mineral-solution reactions that may occur in the aquifer. Considerations were also conducted on the concentrations of the reactive gases H_2S, H_2 and CO_2 in relation to their approach to equilibrium with respect to selected mineral-gas reactions.

The modelled aquifer chemistry exposed the existence of a wide-ranging difference in composition between aquifer and discharged wellhead waters with a general increase in the contents of most elements at surface conditions. The results indicate that the aquifer fluid in Domes is characterized by Na-Cl-HCO_3 water types, with a pH range of between 5.97 and 7.73. Two of the samples (OW-904B and OW-909) gave relatively anomalously high pH (>7.0). Liquid water enthalpies calculated for the initial aquifer conditions were, by and large, below 1000 kJ/kg with an exception of noted wells.

However, the discharge enthalpies were in excess and correspond to a vapour-dominated system in terms of volume, as opposed to the calculated water enthalpy of the aquifer, showing excesses of between 13 and 54% to the measured enthalpy. Concentrations of Cl in the aquifer varied from 152 to 867 mg/kg compared to HCO_3 (380 to 2333 mg/kg), a phenomenon uncharacteristic of high-temperature geothermal systems. Such high HCO_3 values can either be indicative of a peripheral origin of aquifer water or high levels of magma degassing causing high CO_2 flux. The latter is suggested to be the cause of anomalous HCO_3 content. Among the cations, Na gave high values, i.e., 261-578 mg/kg, when compared to K, Ca and Mg, The average values for K, Ca and Mg were 70, 1.1 and 0.22 mg/kg, respectively. The amount of SiO_2 in the aquifer water varied from 216 to 614 mg/kg with an increase in a range of 13-40% in the measured SiO_2 from the discharge fluids.

Reactive gas species, H_2S, H_2 and CO_2, provide information on the physical state of geothermal reservoirs such as temperature and steam-to-water ratio. Two mineral assemblages were selected for CO_2 concentrations. Apart from three samples showing a scatter closely matching the assemblages, they were generally higher, averaging 0.3 to 0.4 SI units with reference to clinozoisite-calcite-quartz-prehnite and clinozoisite-calcite-quartz-grossular mineral assemblages, respectively. The CO_2 concentrations were considerably high, attributable to a high flux of this gas from the magmatic source which hinders its close approach to local equilibrium with the mineral assemblages considered.

Three mineral assemblages were selected for H_2S and, in general, the aquifer water showed that the content of this gas was low relative to the equilibrium of the assemblages, with an average of -1.0, -0.7 and -0.5 SI units, respectively. Further separate assessment of the aquifer waters revealed that three of the samples related closely to the assemblages. It is more likely that the relatively low amount of H_2S is due to oxidation or contamination of samples with atmospheric air. Although O_2 was not detected in these waters, as reported in the discharge data, it could have been initially present but then subsequently destroyed by reaction with H_2S in the alkaline medium of the NaOH-solution upon sample storage. The H_2 concentrations in these calculated aquifer fluids displayed a considerable scatter, showing no relationships with CO_2 and H_2S, with respect to the three assemblages selected. On average, the departure of H_2 from mineral equilibrium with assemblages 6, 7 and 8, was on the magnitude of -0.05, -0.4 and 1.2, respectively. A single sample showed a close relationship with the hem-mag assemblage whereas the rest displayed indistinct dispersion across pyrr-pyr-mag and gro-pyrr-qtz-epi-wol-pyr mineral assemblages.

The ion activity product for calcite (Q) in aquifer waters of individual wells was scattered around the solubility constant for calcite. The average departure from equilibrium was 0.07 log (Q/K) units and the standard deviation 0.62 log (Q/K) units. Some samples were far from saturated, in particular from wells OW-901 and OW-903A. The graph for fluorite shows that the aquifer waters of the lowest temperature were very close to being fluorite saturated while hotter waters were under-saturated. In all of the aquifer waters considered for the present study, the dominant fluoride species was F^-. The other important F^-species was HF^o but it only constituted a small fraction of the dissolved F in all cases. The fluoride concentrations in the various aquifer waters were very variable. Based on the data on the F-species and the data for calcite, it was concluded that most of the aquifer waters modelled here are truly fluorite under-saturated.

LogQ values for calcite changed from under-saturation to over-saturation with increasing aquifer water pH. This change was not considered to be real, but rather an artefact reflecting an error in the calculated aquifer water pH. Equilibration between an aqueous solution and calcite is rapidly attained, certainly at the high temperatures of the Olkaria reservoir. The values calculated for aquifer water calcite saturation is dependent on several factors, largely the measured pH of water samples, and the analyzed concentrations of total carbonate carbon, also in water samples and the selection of aquifer water temperature. Errors in these parameters were considered to also be the cause of the observed relationship between the degree of calcite saturation and pH.

To delineate a conceptual model of the well field, understanding the depth level and behaviour of feed

zones was an essential step in this study. Pressure and temperature logs, circulation losses and geothermometer results from respective wells combined to establish the location of such zones in Domes. The downhole pressure and temperature profiles obtained during the transient warm-up state of the wells were a valuable investment, providing imperative information that might not be obtainable once the system has been altered by discharge. Nonetheless, the discussion here is restricted to wells with available data.

It is very clear from the temperature logs that most of the discharged wells considered had not thermally stabilized at the end of downhole measurements. The feed zones were evaluated based on downhole temperature response to heating of the well. This assessment was done with reference to the boiling point curve as well as the consistency of the runs. The boiling point curve was drawn from the water table depth in respective wells and varied from 360 to 600 m, averaging at 480 m below the surface. The water table depths were taken from the pressure logs. The wells that approached thermal stability, at least at a certain depth of the well, included wells OW-907A, OW-912, OW-914 and OW-915A. The rest of the wells were still in flux by the time the final runs were conducted. However, from the assessment, the majority of the wells are either sub-boiling or with two phases, as some wells had heated sufficiently to reach the boiling point curve.

At feed zone depth levels, there is direct contact between the well fluid and the reservoir, where the pressure in the well is equal to that at the same level in the reservoir. As the well heats up, a transient decay of pressure build-up caused by injection, and a change in gradient caused by the warming of the water column in the well, occur. Pressure tends to pivot at these points where separate pressure runs converge. The present study utilized pressure logs to identify pressure pivots in the well and, thus, horizons that control well pressures. For some wells, pivoting was seen to occur between two or even more feed zones at depth, suggesting comparable pressure potential in different horizons. Shifting of pressure potential was also common, possibly a result of reopening or closing of aquifers during pressure build-up. Examined pressure logs indicated that the pivot zones occurred at depths varying between 1050 and 2500 m below the surface.

The losses or gains of the circulation of drilling fluids are indicative of permeable zones. However, reports of circulation losses available for the present study were limited and unreliable. They were limited in the sense that the data available were not sufficient for spatial analysis, and unreliable in the sense that most were not reported alongside drilling reports as a complement to geological observation in assessing circulation loss. From the results, it was apparent that some shallow permeable zones had been cased off. Nevertheless, deep-seated permeable zones below the casing were noted. Geothermometer temperatures obtained from the WATCH chemical speciation program were used alongside pressure logs to identify depth levels of dominating producing horizons based on the assumption that the temperature in the formation followed the boiling point curve with depth. Geothermometer temperatures diverged by more than 100°C. The lowest aquifer temperature from a geothermometer reading was 204°C and the highest was 321°C, averaging at about 249°C. The corresponding depths of these temperatures varied from 700 to 2000 m.

The combined use of geothermometers, measured enthalpy, selected aquifer depths and subsurface pressure distribution from the selected reference depths, and weighing the results against the outputs led to a conceptual model of the field. The depiction suggested that producing horizons deepened towards the east and southeast segments of the well field and the deeper these producing horizons the better the outputs. The high pressure, deeper feeding horizons and high enthalpy correlate with high output of wells. With this model, the erection of a 2×70 MWe power plant within the well field becomes more likely; as the data already indicate that a 120 MWe (~80%) has been proven possible, and assuming a surplus of 10% as the trend suggests, then populating the eastern sector with strategic wells may bring the plan to fruition soon.

In conclusion, the full potential of Domes well field has yet to be realized. Understanding the distribution of the chemical components within the reservoir and, hence, their characteristics, has been

successfully concluded, despite data limitation. The presented conceptual model is but a preliminary observation; unfolding outcomes from ongoing developments in the field will refine this concept. As a recommendation, further well flow tests, followed by a comprehensive numerical simulation, is the next most preferable step in outlining the extent of the productive area within Domes well field.

ACKNOWLEDGMENTS

My heartfelt gratitude and sincere appreciation go to the Government of Iceland in collaboration with the United Nations University Geothermal Training Programme (UNU-GTP) for awarding me UNU Fellowship under the esteemed stewardship and help of Dr. Ingvar B. Fridleifsson (Director) and Mr. Lúdvík S. Georgsson (Deputy Director). I am also grateful to Ms. Thórhildur Ísberg, Ms. Dorthe H. Holm, and Mr. Ingimar G. Haraldsson and Markús A.G. Wilde, staff of UNU-GTP, for their heartfelt kindness. I am indebted to Prof. Stefán Arnórsson for his warm supervision and the overwhelming advice he accorded me during the preparation of this report. Special thanks to my employer, Geothermal Development Company - GDC for granting me the memorable chance to undertake this study. I would also like to acknowledge Kenya Electricity Generating Company Ltd. – KenGen, for availing the data without which this study would not have been successful. Finally, to God: 'Eben hà-ezer this far.

REFERENCES

Ambusso, W.J., and Ouma, P.A., 1991: Thermodynamic and permeability structure of Olkaria northeast field: Olkaria fault. *Geothermal Resource Council, Transactions, 15*, 237-242.

Angcoy, E.L., and Arnórsson, S., 2010: An experiment on monomeric and polymeric silica precipitation rates from supersaturated solutions. *Proceedings of World Geothermal Congress 2010, Bali, Indonesia,* 6 pp.

Arnórsson, S., 2000: Reactive and conservative components. In: Arnórsson, S. (editor), *Isotopic and chemical techniques in geothermal exploration, development and use.* IAEA, Vienna, 40-48.

Arnórsson, S., and Stefánsson, A., 2005: Wet-steam well discharges. II. Assessment of aquifer fluid compositions. *Proceedings of the World Geothermal Congress 2005, Antalya, Turkey,* 11 pp.

Arnórsson, S., Stefánsson, A., and Bjarnason, J.Ö, 2007: Fluid-fluid interaction in geothermal systems. *Reviews in Mineralogy & Geochemistry, 65*, 259-312.

Arnórsson, S., Sigurdsson, S., and Svavarsson, H., 1982: The chemistry of geothermal waters in Iceland. I. Calculation of aqueous speciation from 0° to 370°C. *Geochim. Cosmochim. Acta*, *46*, 1513–1532.

Arnórsson, S., Angcoy, E., Bjarnason, J.Ö., Giroud, N., Gunnarsson, I., Kaasalainen, H., Karingithi, C., and Stefánsson, A., 2010: Gas chemistry of volcanic geothermal systems. *Proceedings of World Geothermal Congress 2010, Bali, Indonesia,* 12 pp.

Baker, B.H., and Wohlenberg, J., 1971: Structural evolution of the Kenya Rift Valley. *Nature*, *229*, 538-542.

Baker, B.H., Mohr, P.A., and Williams, L.A.J., 1972: *Geology of the eastern rift system of Africa*. Geological Society of America, Special Paper 136, 67 pp.

Baker, B.H., Williams, L.A.J., Miller, J.A., and Fitch, F.J., 1971: Sequence and geochronology of the Kenya Rift volcanics. *Tectonophysics, 11,* 191-215.

Bjarnason, J.Ö., 2010: *The speciation program WATCH, Version 2.4, user's guide*. The Iceland water chemistry group, Reykjavik, 9 pp.

Busey, R.H., and Mesmer, R.E., 1977: Ionization equilibria of silicic-acid and polysilicate formation in aqueous sodium chloride solutions to 300°C. *Inorg. Chem., 16*, 2444–2450.

Clarke, M.C.G., Woodhall, D.G., Allen, D., and Darling, G., 1990: *Geological, volcanological and hydogeological controls of the occurrence of geothermal activity in the area surrounding Lake Naivasha, Kenya*. Ministry of Energy, report.

Fernandez-Prini, R., Alvarez, J.L., and Harvey, A.H., 2003: Henry´s constants and vapour-liquid distribution constants for gaseous solutes in H_2O and D_2O at high temperatures. *J. Phys. Chem. Ref. Data*, *32*, 903-916.

Grant, M.A., Donaldson, I.G., and Bixley, P.F., 1982: *Geothermal reservoir engineering*. Academic Press, NY, 369 pp.

Gudmundsson, B.T., and Arnórsson, S., 2005: Secondary mineral fluid equilibria in the Krafla and Námafjall geothermal systems, Iceland. *Appl. Geochem*., *20*, 1607-1625.

Gunnarsson, I., and Arnórsson, S., 2005: Impact of silica scaling on the efficiency of heat extraction from high-temperature geothermal fluids. *Geothermics, 34*, 320–329.

Holland, T.J.B., and Powell, R., 1998: An internally consistent thermodynamic data set for phases of petrological interest. *J. Metamorph. Geol*., *16*, 309–343.

Karingithi, C.W, Arnórsson, S., and Grönvold, K., 2010: Processes controlling aquifer fluid compositions in the Olkaria geothermal system, Kenya. *J. Volcanol. & Geoth. Res., 196,* 57-76.

Kariuki, M.N., 2003: Reservoir assessment and wellbore simulations for the Olkaria domes geothermal field, Kenya. Report 14 in: *Geothermal Training in Iceland 2003.* UNU-GTP, Iceland, 337-360.

KenGen, 1998: *Surface exploration of Kenya's geothermal resources in the Kenya Rift.* The Kenya Electricity Generating Company, Ltd, internal report, 84 pp.

KenGen, 2000: *Conceptualized model of Olkaria geothermal field.* The Kenya Electricity Generating Company, Ltd, internal report, compiled by Muchemi, G.G., 13 pp.

Lagat, J.K., 1995: Borehole geology and hydrothermal alteration of well OW-30, Olkaria geothermal field, Kenya. Report 6 in: *Geothermal Training in Iceland 1995.* UNU-GTP, Iceland, 135-154.

Lagat, J.K., 2004: *Geology, hydrothermal alteration and fluid inclusion studies of the Olkaria Domes geothermal field, Kenya*. University of Iceland, MSc thesis, UNU-GTP, Iceland, report 2, 71 pp.

Leaver, J.D., 1986: Injectivity and productivity estimation in multiple feed geothermal wells. *Proceedings of the 11th Workshop on Geothermal Reservoir Engineering, Stanford University, Stanford, Ca,* 6 pp.

Lichoro, C.M., 2009: 1-D inversion of TEM and MT data from Olkaria Domes geothermal area, Kenya. Report 16 in: *Geothermal Training in Iceland 2009.* UNU-GTP, Iceland, 289-318.

Macdonald, R., Davies, G.R., Bliss, C.M., Leat, P.T., Bailey, D.K., and Smith, R.L., 1987: Geochemistry of high silica peralkaline rhyolites, Naivasha, Kenya rift valley. *Petrology, 28*, 979-1008.

Malimo, S.J., 2009: Interpretation of geochemical well test data for wells OW-903B, OW-904B and OW-909 Olkaria Domes, Kenya. Report 17 in: *Geothermal Training in Iceland 2009.* UNU-GTP, Iceland, 319-344.

Muchemi, G.G., 1999: *Conceptualised model of the Olkaria geothermal field*. The Kenya Electricity Generating Company Ltd*., internal report,* 46 pp.

Mungania, J., 1992: *Preliminary field report on geology of Olkaria volcanic complex with emphasis on Domes area field investigations*. Kenya Power Company, internal report.

Mungania J., 1999: *Summary of the updates of the geology of Olkaria Domes geothermal field.* KenGen, internal report.

Ofwona, C.O., 2002: *A reservoir study of Olkaria east geothermal system, Kenya*. University of Iceland, MSc thesis, UNU-GTP, Iceland, report 1, 86 pp.

Ogoso-Odongo, M.E., 1986: Geology of Olkaria geothermal field. *Geothermics*, *15*, 741-748.

Omenda, P.A., 1994: The geological structure of the Olkaria west geothermal field, Kenya. *Proceedings of the 19th Workshop on Geothermal Reservoir Engineering, Stanford University, Stanford, Ca,* 125-130.

Omenda, P.A., 1998: The geology and structural controls of the Olkaria geothermal system, Kenya. *Geothermics*, 27, 55-74.

Omenda, P.A., 2000: Anatectic origin for comendite in Olkaria geothermal field, Kenya Rift; Geochemical evidence for syenitic protholith. *African J. of Science and Technology, Science and Engineering series, 1*, 39-47.

Opondo, K.M., 2008: Fluid characteristics of three exploration wells drilled at Olkaria Domes field, Kenya. *Proceedings of the 33rd Workshop on Geothermal Reservoir Engineering, Stanford University, Stanford, Ca,* 6 pp.

Renner, J.L., Shook, G.M., Garg, S., Finger, J.T., Kasameyer, P.W., Bloomfield, K.K., Hirtz, P.N., and Mines, G.L., 2007: Geothermal engineering. In: Lake, L.W. (editor-in-chief), *Petroleum engineering handbook.* Society of Petroleum Engineers, 629 pp.

Robie, R.A., and Hemingway, B.S., 1995: Thermodynamic properties of minerals and related substances at 298.15 K and 1 bar (10^5 Pascals) pressures and at higher temperatures. *U.S.G.S. Bull.*, *2131*, 461 pp.

Shackleton, R.M., 1986: Precambrian collision tectonics in Africa. In: Coward, M.P., and Ries, A.C. (editors), *Collision tectonics.* Geol. Soc., Spec. Publ., 19, 329-349.

Simiyu, S.M., and Keller, G.R., 1997: An integrated analysis of lithospheric structure across the East African plateau based on gravity anomalies and recent seismic studies. *Tectonophysics*, *278*, 291-313.

Simiyu, S.M., Oduong, E.O., and Mboya, T.K., 1998: *Shear wave attenuation beneath the Olkaria volcanic field.* KenGen, internal report.

Smith, M., 1994: Stratigraphic and structural constraints on mechanisms of active rifting in the Gregory Rift, Kenya. *Tectonophysics, 236*, 3-22.

Smith, M., and Mosley, P., 1993: Crustal heterogeneity and basement influence on the development of the Kenya rift, East Africa. *Tectonics*, *12-2,* 591-606.

Spichak, V.V., and Zakharova, O.K., 2009: Electromagnetic temperature extrapolation in depth in the Hengill geothermal area, Iceland. *Proceedings of the 34th Workshop on Geothermal Reservoir Engineering, Stanford University, Stanford, Ca*, 6 pp.

Tossell, J.A., and Sahai, N., 2000: Calculating the acidity of silanols and related oxyacids in aqueous solution. *Geochim. Cosmochim. Acta, 64*, 4097–4113.

Williams, L.A.J., 1972: The Kenya rift volcanics: a note on volumes and chemical composition. *Tectonophysics*, *15,* 83-96.

Zotov, N., and Keppler, H., 2002: Silica speciation in aqueous fluids at high pressures and high temperatures, *Chemical Geology*, *184,* 71-82.

APPENDIX I: Pressure and temperature profiles from Olkaria Domes well field

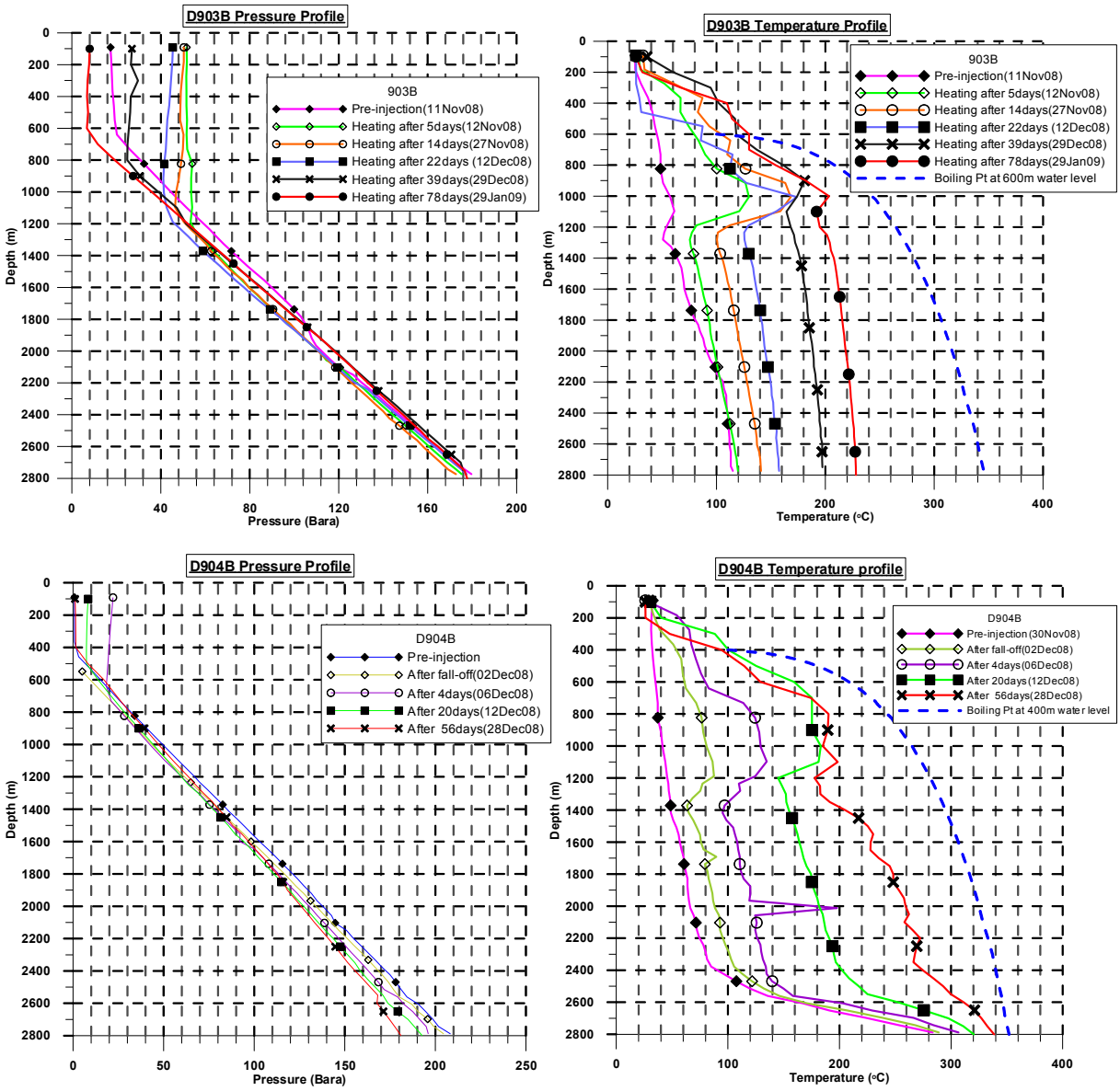

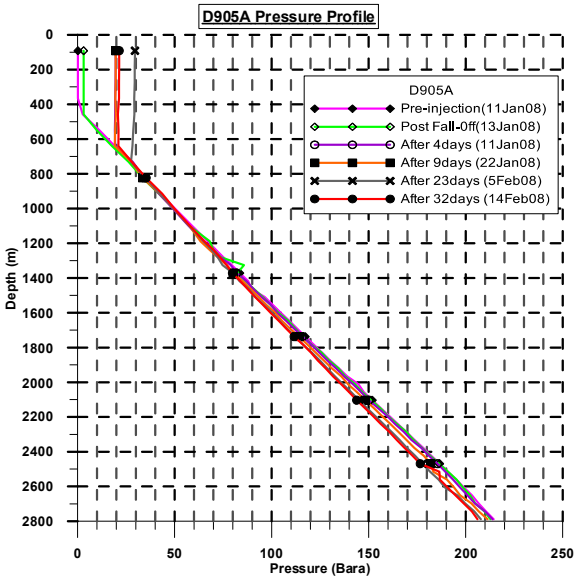
D905A Pressure Profile
D905A
Pre-injection(11Jan08)
Post Fall-0ff(13Jan08)
After 4days (11Jan08)
After 9days (22Jan08)
After 23days (5Feb08)
After 32days (14Feb08)
Depth (m)
Pressure (Bara)

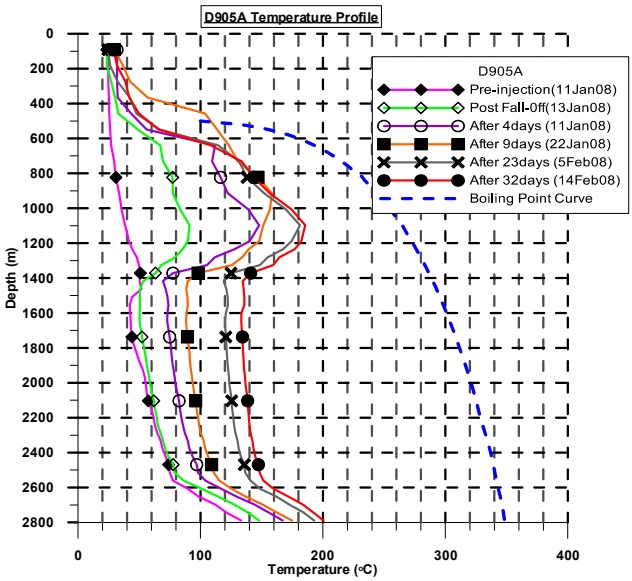
D905A Temperature Profile
D905A
Pre-injection(11Jan08)
Post Fall-0ff(13Jan08)
After 4days (11Jan08)
After 9days (22Jan08)
After 23days (5Feb08)
After 32days (14Feb08)
Boiling Point Curve
Depth (m)
Temperature (°C)

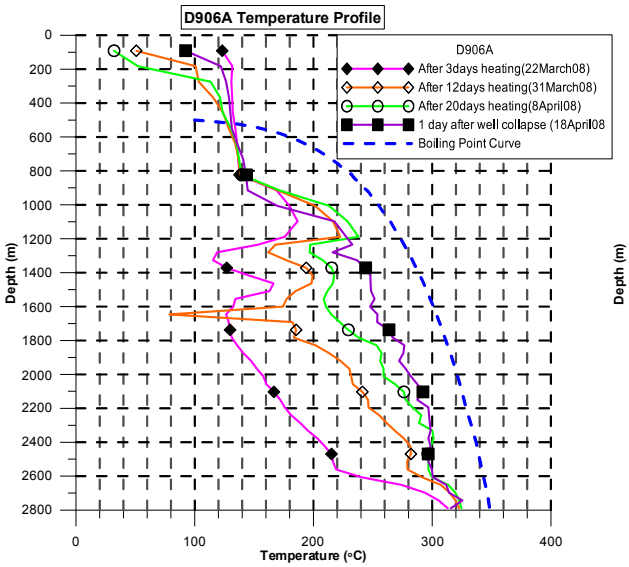
D906A Temperature Profile
D906A
After 3days heating(22March08)
After 12days heating(31March08)
After 20days heating(8April08)
1 day after well collapse (18April08
Boiling Point Curve
Depth (m)
Temperature (°C)

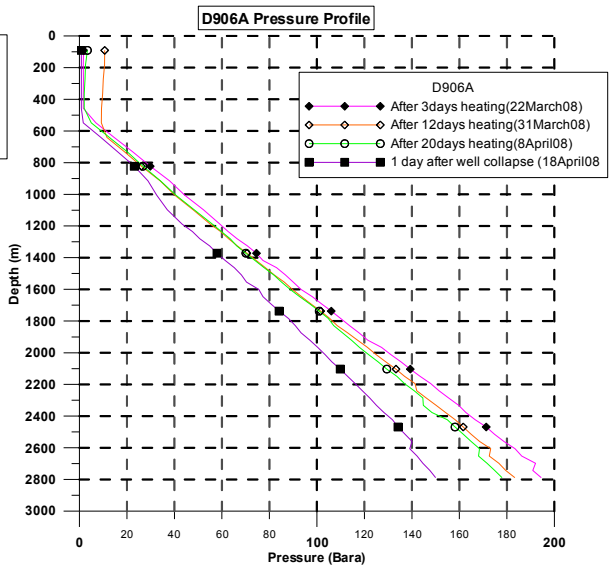
D906A Pressure Profile
D906A
After 3days heating(22March08)
After 12days heating(31March08)
After 20days heating(8April08)
1 day after well collapse (18April08
Depth (m)
Pressure (Bara)

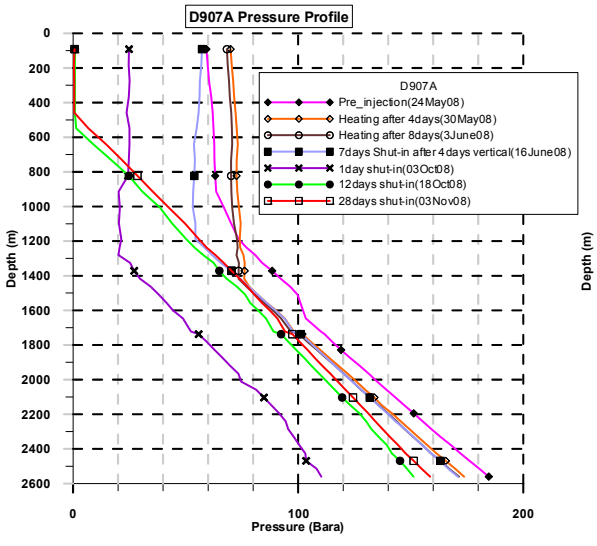
D907A Pressure Profile
D907A
Pre_injection(24May08)
Heating after 4days(30May08)
Heating after 8days(3June08)
7days Shut-in after 4days vertical(16June08)
1day shut-in(03Oct08)
12days shut-in(18Oct08)
28days shut-in(03Nov08)
Depth (m)
Pressure (Bara)

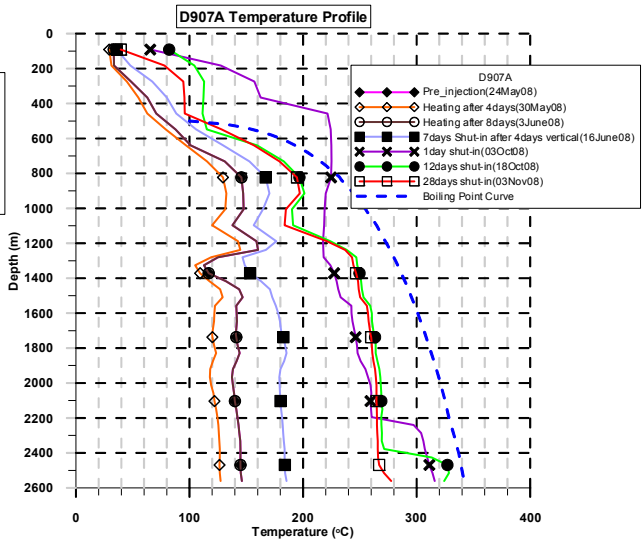
D907A Temperature Profile
D907A
Pre_injection(24May08)
Heating after 4days(30May08)
Heating after 8days(3June08)
7days Shut-in after 4days vertical(16June08)
1day shut-in(03Oct08)
12days shut-in(18Oct08)
28days shut-in(03Nov08)
Boiling Point Curve
Depth (m)
Temperature (°C)

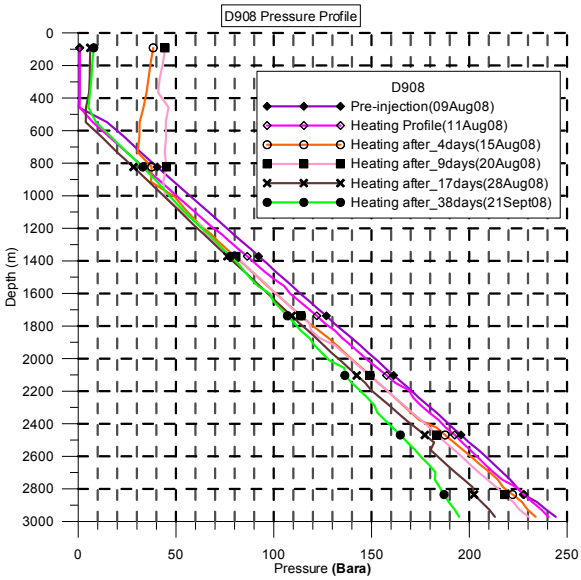
D908 Pressure Profile
D908
Pre-injection(09Aug08)
Heating Profile(11Aug08)
Heating after_4days(15Aug08)
Heating after_9days(20Aug08)
Heating after_17days(28Aug08)
Heating after_38days(21Sept08)
Depth (m)
Pressure (Bara)

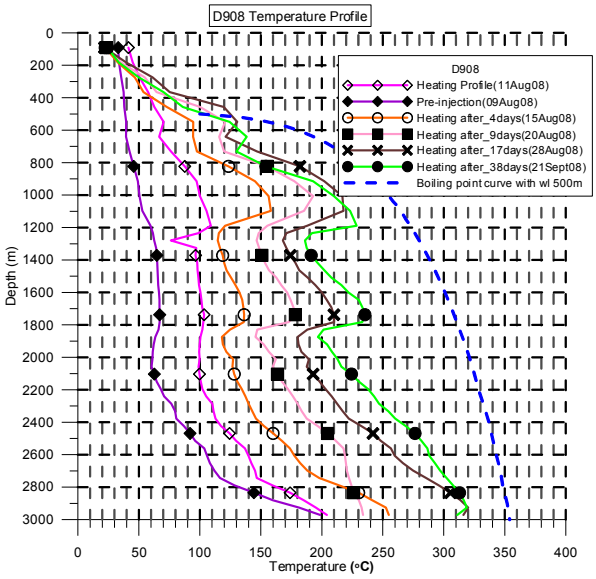
D908 Temperature Profile
D908
Heating Profile(11Aug08)
Pre-injection(09Aug08)
Heating after_4days(15Aug08)
Heating after_9days(20Aug08)
Heating after_17days(28Aug08)
Heating after_38days(21Sept08)
Boiling point curve with wl 500m
Depth (m)
Temperature (°C)

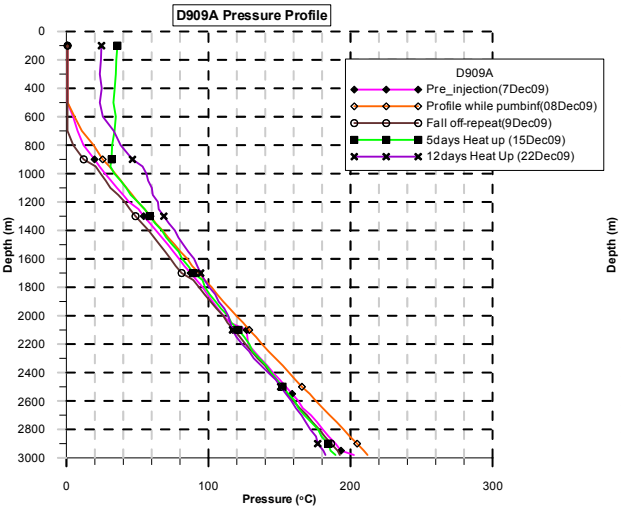
D909A Pressure Profile
D909A
Pre_injection(7Dec09)
Profile while pumbinf(08Dec09)
Fall off-repeat(9Dec09)
5days Heat up (15Dec09)
12days Heat Up (22Dec09)
Depth (m)
Pressure (°C)

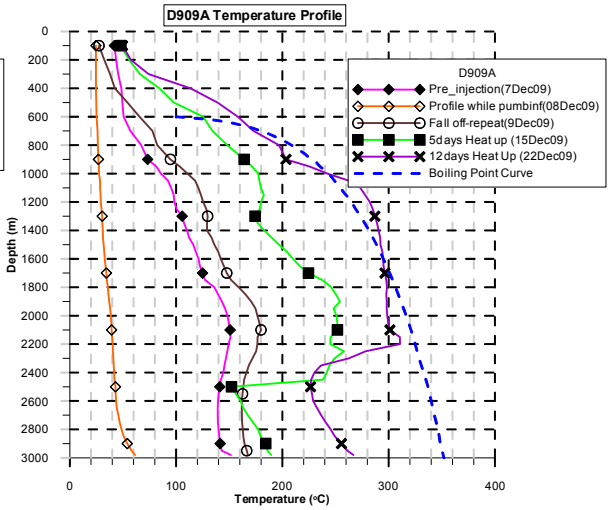
D909A Temperature Profile
D909A
Pre_injection(7Dec09)
Profile while pumbinf(08Dec09)
Fall off-repeat(9Dec09)
5days Heat up (15Dec09)
12days Heat Up (22Dec09)
Boiling Point Curve
Depth (m)
Temperature (°C)

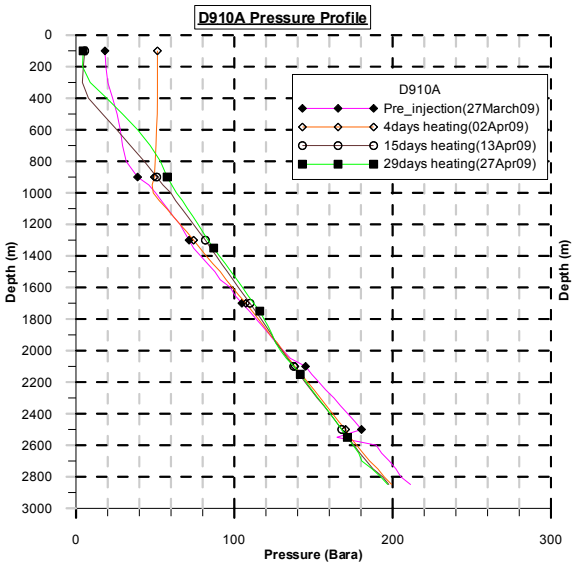
D910A Pressure Profile
D910A
Pre_injection(27March09)
4days heating(02Apr09)
15days heating(13Apr09)
29days heating(27Apr09)
Depth (m)
Pressure (Bara)

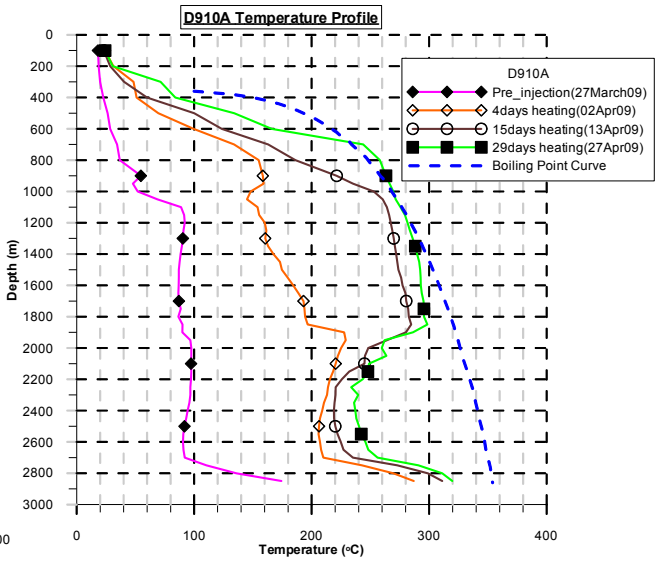
D910A Temperature Profile
D910A
Pre_injection(27March09)
4days heating(02Apr09)
15days heating(13Apr09)
29days heating(27Apr09)
Boiling Point Curve
Depth (m)
Temperature (°C)

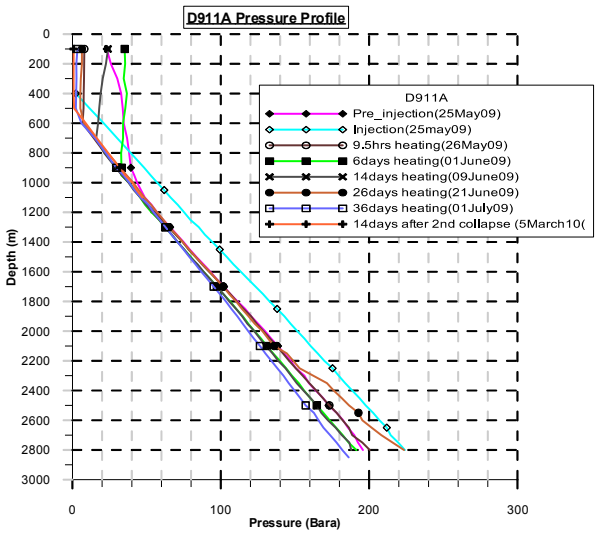
D911A Pressure Profile
D911A
Pre_injection(25May09)
Injection(25may09)
9.5hrs heating(26May09)
6days heating(01June09)
14days heating(09June09)
26days heating(21June09)
36days heating(01July09)
14days after 2nd collapse (5March10(
Depth (m)
Pressure (Bara)

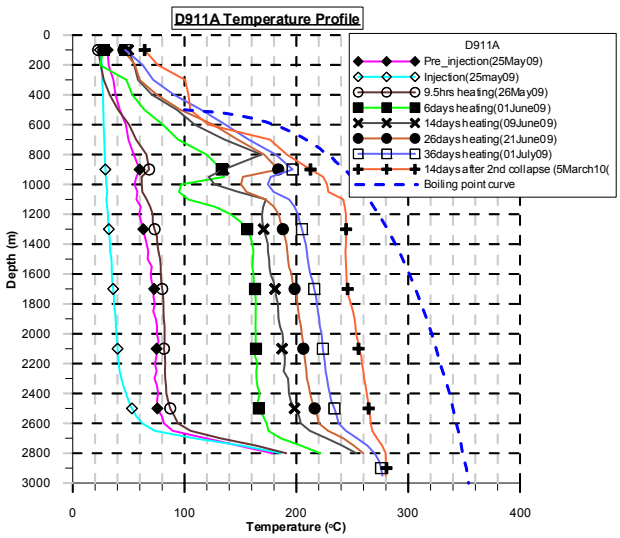
D911A Temperature Profile
D911A
Pre_injection(25May09)
Injection(25may09)
9.5hrs heating(26May09)
6days heating(01June09)
14days heating(09June09)
26days heating(21June09)
36days heating(01July09)
14days after 2nd collapse (5March10(
Boiling point curve
Depth (m)
Temperature (°C)

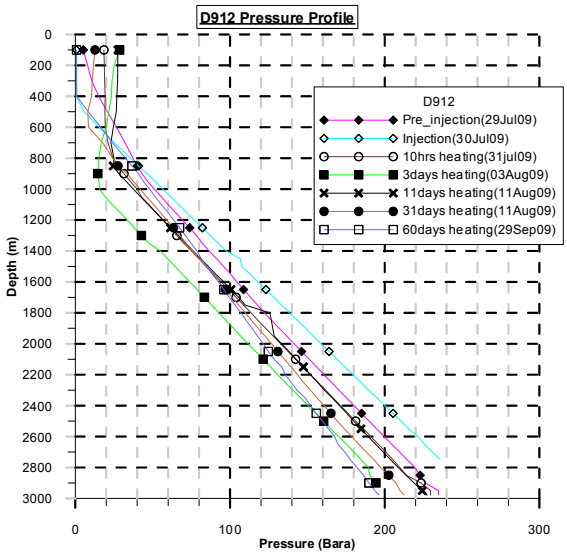
D912 Pressure Profile
D912
Pre_injection(29Jul09)
Injection(30Jul09)
10hrs heating(31jul09)
3days heating(03Aug09)
11days heating(11Aug09)
31days heating(11Aug09)
60days heating(29Sep09)
Depth (m)
Pressure (Bara)

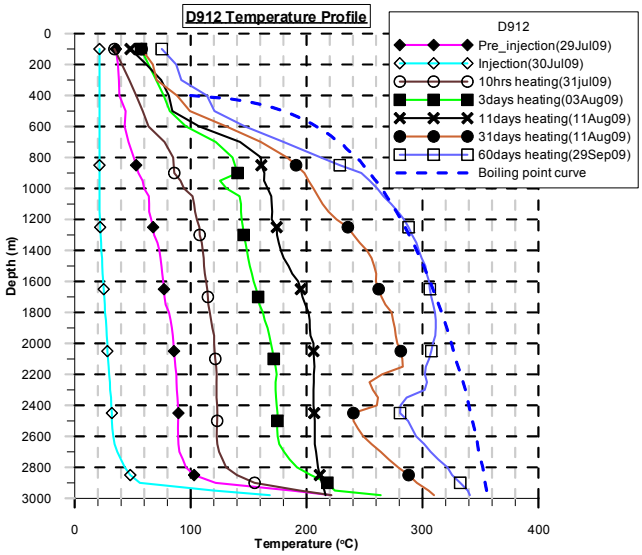
D912 Temperature Profile
D912
Pre_injection(29Jul09)
Injection(30Jul09)
10hrs heating(31jul09)
3days heating(03Aug09)
11days heating(11Aug09)
31days heating(11Aug09)
60days heating(29Sep09)
Boiling point curve
Depth (m)
Temperature (°C)

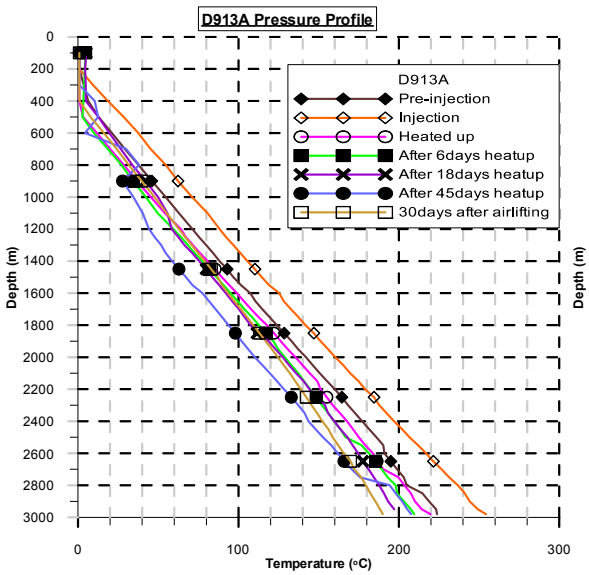
D913A Pressure Profile
D913A
Pre-injection
Injection
Heated up
After 6days heatup
After 18days heatup
After 45days heatup
30days after airlifting
Depth (m)
Temperature (°C)

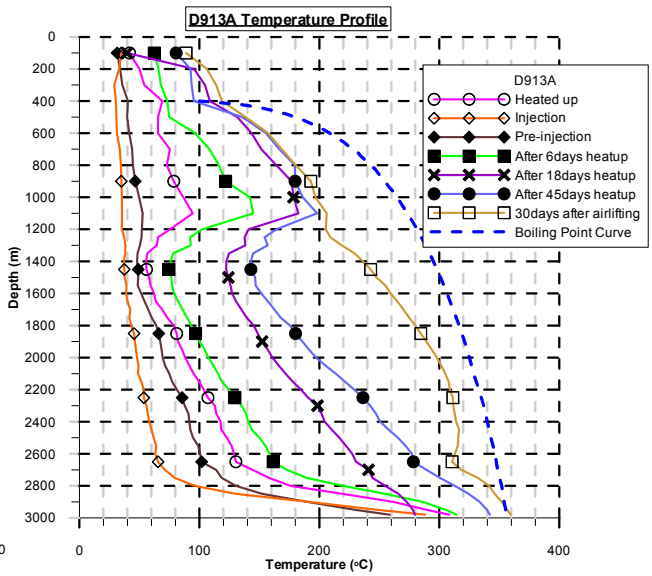
D913A Temperature Profile
D913A
Heated up
Injection
Pre-injection
After 6days heatup
After 18days heatup
After 45days heatup
30days after airlifting
Boiling Point Curve
Depth (m)
Temperature (°C)

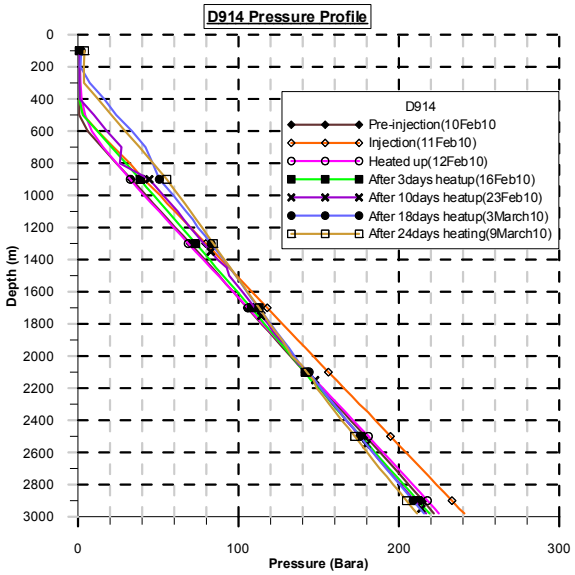
D914 Pressure Profile
Depth (m)
Pressure (Bara)
D914
Pre-injection(10Feb10
Injection(11Feb10)
Heated up(12Feb10)
After 3days heatup(16Feb10)
After 10days heatup(23Feb10)
After 18days heatup(3March10)
After 24days heating(9March10)

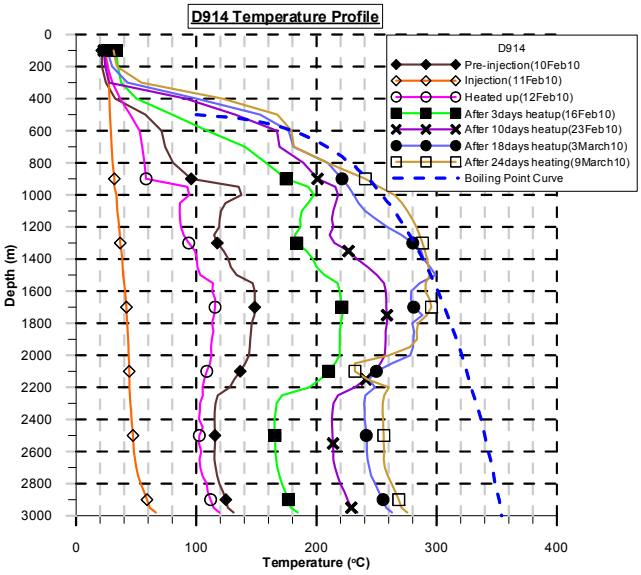
D914 Temperature Profile
Depth (m)
Temperature (°C)
D914
Pre-injection(10Feb10
Injection(11Feb10)
Heated up(12Feb10)
After 3days heatup(16Feb10)
After 10days heatup(23Feb10)
After 18days heatup(3March10)
After 24days heating(9March10)
Boiling Point Curve

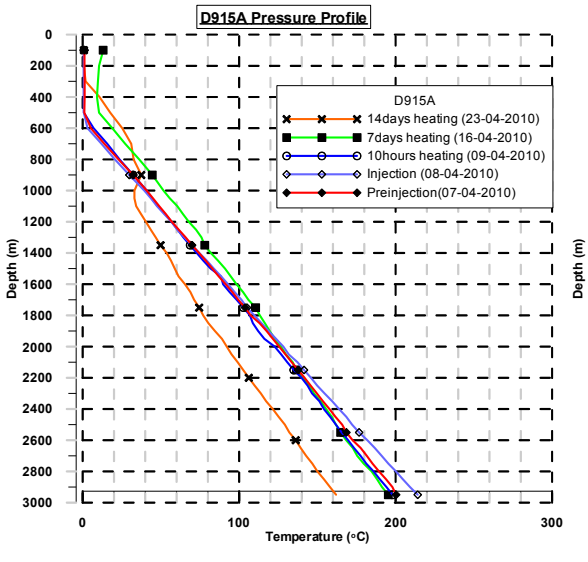
D915A Pressure Profile
Depth (m)
Temperature (°C)
D915A
14days heating (23-04-2010)
7days heating (16-04-2010)
10hours heating (09-04-2010)
Injection (08-04-2010)
Preinjection(07-04-2010)

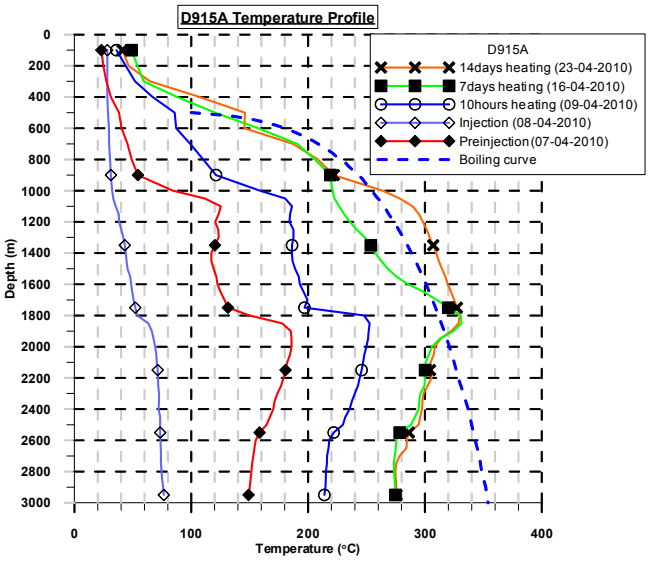
D915A Temperature Profile
Depth (m)
Temperature (°C)
D915A
14days heating (23-04-2010)
7days heating (16-04-2010)
10hours heating (09-04-2010)
Injection (08-04-2010)
Preinjection(07-04-2010)
Boiling curve

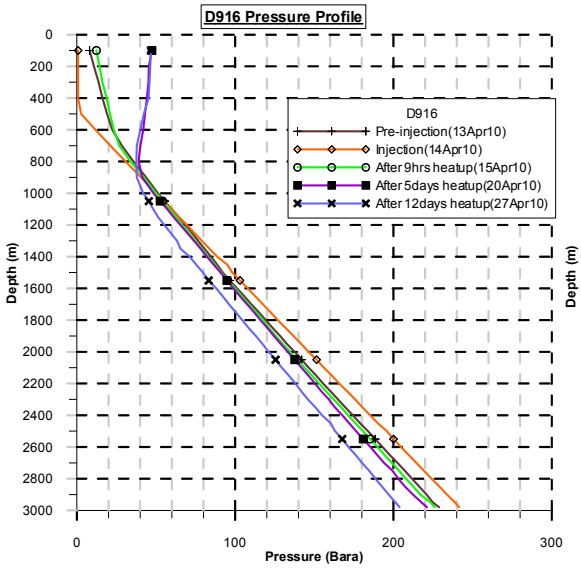
D916 Pressure Profile
Depth (m)
Pressure (Bara)
D916
Pre-injection(13Apr10)
Injection(14Apr10)
After 9hrs heatup(15Apr10)
After 5days heatup(20Apr10)
After 12days heatup(27Apr10)

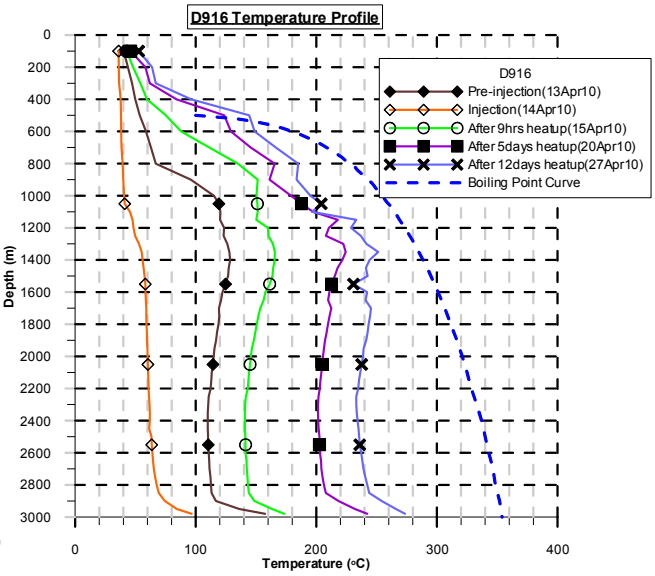
D916 Temperature Profile
Depth (m)
Temperature (°C)
D916
Pre-injection(13Apr10)
Injection(14Apr10)
After 9hrs heatup(15Apr10)
After 5days heatup(20Apr10)
After 12days heatup(27Apr10)
Boiling Point Curve